PL-TR-97-2067

HIGH RESOLUTION MOLECULAR SPECTROSCOPY OF CO_2 AND H_2O

Mark P. Esplin
Richard B. Wattson
Ronald J. Huppi

Stewart Radiance Laboratory
139 The Great Road
Bedford, MA 01730

June 1997

Final Report
1 March 1990 to 1 June 1997

Approved for public release; distribution unlimited

PHILLIPS LABORATORY
Directorate of Geophysics
AIR FORCE MATERIEL COMMAND
HANSCOM AFB, MA 01731-3010

This technical report has been reviewed and is approved for publication.

Michael Hoke
Michael Hoke
Contract Manager

Laila Jeong
Laila Jeong, Chief
Background Clutter Mitigation Branch

William A.M. Blumberg
William A.M. Blumberg, Director
Optical Effects Division

This report has been reviewed by the ESC Public Affairs Office (PA) and is releasable to the National Technical Information Service (NTIS).

Qualified requestors may obtain additional copies from the Defense Technical Information Center (DTIC). All others should apply to the National Technical Information Service (NTIS).

If you address has changed, if you wish to be removed from the mailing list, or if the addressee is no longer employed by your organization, please notify PL/IM, 29 Randolph Road, Hanscom AFB, MA 01731-3010. This will assist us in maintaining a current mailing list.

Do not return copies of this report unless contractual obligations or notices on a specific document require that it be returned.

REPORT DOCUMENTATION PAGE

Form Approved
OMB No. 0704-0188

1. AGENCY USE ONLY *(Leave blank)*	2. REPORT DATE	3. REPORT TYPE AND DATES COVERED
	June 1997	Final, 1 March 1990-1 June 1997

4. TITLE AND SUBTITLE
High Resolution Molecular Spectroscopy of CO_2 and H_2O

5. FUNDING NUMBERS
PE 61102F
PR 2310 TA G1 WU CA

Contract F19628-90-K-0016

6. AUTHOR(S)
Mark P. Esplin
Richard B. Wattson
Ronald J. Huppi

7. PERFORMING ORGANIZATION NAME(S) AND ADDRESS(ES)
Stewart Radiance Laboratory
139 The Great Road
Bedford, MA 01730

8. PERFORMING ORGANIZATION REPORT NUMBER

9. SPONSORING/MONITORING AGENCY NAME(S) AND ADDRESS(ES)
Phillips Laboratory
29 Randolph Road
Hanscom AFB, MA 01731-3010

Contract Manager: Michael Hoke/GPOS

10. SPONSORING/MONITORING AGENCY REPORT NUMBER
PL-TR-97-2067

11. SUPPLEMENTARY NOTES

12a. DISTRIBUTION/AVAILABILITY STATEMENT
Approved for public release, distribution unlimited

12b. DISTRIBUTION CODE

13. ABSTRACT *(Maximum 200 words)*

The Air Force Geophysics Directorate high resolution Michelson interferometer and high temperature absorption cell were used to study the infrared absorption spectra of CO_2 and H_2O. Gas samples were heated to temperatures as high as 1000 K. Over 12,000 molecular transitions were identified in the experimental spectra. Line position for these transitions have been measured with an accuracy up to 0.0004 cm^{-1}. In order to identify these molecular transitions in the crowded high temperature experimental spectra, several data analysis techniques were developed. In addition, the servo system that controls the high resolution interferometer was enhanced to increase its reliability and stability.

14. SUBJECT TERMS
infrared, spectroscopy, carbon dioxide, water vapor, high temperature, Michelson interferometer

15. NUMBER OF PAGES
58

16. PRICE CODE

17. SECURITY CLASSIFICATION OF REPORT	18. SECURITY CLASSIFICATION OF THIS PAGE	19. SECURITY CLASSIFICATION OF ABSTRACT	20. LIMITATION OF ABSTRACT
Unclassified	Unclassified	Unclassified	SAR

Table of Contents

1. Introduction

Absorption by the CO_2 and H_2O molecules dominate the infrared transmission spectrum of the atmosphere. Knowledge resulting from the research carried out under this contract has contributed to our understanding of several different atmospheric phenomenon. The global heat balance of the atmosphere is dominated by absorption and emission of H_2O and CO_2, the so call "greenhouse" effect. A detailed knowledge of the spectra of the major atmosphere molecules, also makes it possible to detect the spectral contribution of minor atmospheric species. An additional application of this knowledge is detecting high temperature targets through the atmosphere. As part of this contractual effort, over 12,000 molecular transitions frequencies of CO_2 and H_2O were measured and submitted for inclusion in the PL/GPOS HITRAN molecular database. The HITRAN database is used by the U.S. Air Force's atmospheric transmission computer codes and by the atmospheric community.

2. Instrumentation Description

The experimental measurements were made using the Air Force Geophysics Laboratory high resolution Michelson interferometer (1, 2) and high temperature absorption cell (3). The high resolution interferometer is a step-and-hold Michelson interferometer employing cat's eye retro-reflectors for both the moving and fixed mirrors. A maximum optical path of 114 cm was used, resulting in an apodized resolution of 0.009 cm^{-1}. The 1.75 m path stainless-steel high temperature absorption cell is housed in a commercial electric furnace which can be heated to a maximum of 1000 K. Instrument control, data acquisition, and data processing were performed using personal computers running custom software. The spectrometer and absorption cell has been described previously (1, 2). During the course of this contract, the computer controlled servo system that controls the moving cat's eye retro-reflector was updated with additional hardware and software.

An additional real time data acquisition board was added to the computer that controls the high resolution spectrometer. This board was actually a complete real time computer with its own microprocessor, analog to digital, and digital to analog converters. It was necessary to modify the control electronics to interface this additional computer to the rest of the servo system. Software was written to keep both processors working together to control the motion of the interferometer moveable cat's eye and record the interferogram signals. Software compatibility is much more difficult to achieve for real time control applications that have to interact closely with the hardware, than it is for the more general computational computer applications. These enhancements increased the precision, dependability, and diagnostic capability of the servo system that controls the high resolution spectrometer.

A review of how the computer controlled servo that controls the motion of the movable cat's eye is helpful in understanding the enhancements that were made to the control system. The interferometer is a step-and-hold instrument that uses cat's eye retro-reflectors. The maximum optical path length the interferometer can achieve is more than 1 meter. To achieve these large changes in optical path length while maintaining the necessary optical path length positional accuracy needed for interferometric measurements, the interferometer uses three sources of motion. These three sources are: 1) a mechanical lead screw, similar to that used in a metal working lath, is used to provide large motions, 2) a linear electric motor is used to provide motions of the order of 1 centimeter, and 3) a piezoelectric stack mounted on the secondary of one of the cat's eyes is used to provide very fine optical control. A LVDT (linear variable differential transformer) is used to sense the position of the linear motor and cause the lead screw to turn, maintaining the linear motor in the center of its working range. Fine positional information is obtained from detecting the interference fringes from a HeNe laser.

Before the update to the control system, the lead screw could be moving while data was being acquired and the linear motor was stepping. The linear motor and piezo servos were not able to completely compensate for the vibrations caused by the rotating screw. With the updated software, the screw is not allowed to move independently of the linear motor and piezo stack, but instead is maintained in one position until a block of interferogram data has been acquired and written to the hard disk. Then the screw is activated and the linear motor is brought back to the center of its working range. With the new servo configuration, lead screw motion does not perturb the data taking or the stepping of the interferometer. Problems of backlash and gear slap in this lead screw and its drive train have also been minimized by using the computer to optimize the voltage that drives the lead screw motor. In particular, it has proven very helpful to give the lead screw motor a small reverse pulse at the end of lead screw motion to maintain the gear train under load.

Other additions to the control system of the interferometer were enhanced diagnostics and self-correction for some types of mirror motion problems. The new system, using two data acquisition computers, makes possible continuous monitoring of the interferometer optical path difference. With the old system, the optical path difference could not be monitored at the same time that the infrared data was being acquired. The optical path difference needs to be continually monitored since external vibration can occur at any time. When the computer senses improper holding of the optical path difference, diagnostic information is recorded to the hard disk and the affected data point is remeasured after a short delay to allow any external vibrations to subside.

The data collection and reduction software is organized as a number of small programs instead of one large program. These programs communicate with each other through the headers at the start of each data file. The structure of these headers was

changed from a fixed number of parameters to a variable number of parameters to facilitate future enhancements to the software.

3. Molecular Transition Identification Techniques

Probably the biggest problem in working with the high density spectra, that result from high temperature gases, is making correct line identifications. In making these identifications, a combination of a variety of different techniques proved more useful than any single technique. A computer generated Loomis-Wood diagram proved the most helpful in providing initial identifications. Verification of identifications was accomplished most effectively with combination-difference methods. For the CO_2 molecule, some success was obtained using an automated search through the rotation-vibration parameter space. Computer software was developed to implement each of these identification techniques.

3.1. Looms-Wood Diagrams

A Looms-Wood diagram is used to display spectral information graphically in a manner such that it is easy to pick out the lines belonging to a particular rotation-vibration band or sub-band in the presence of many overlapping bands. A version of the software needed to display Looms-Wood diagrams had been developed previously (4), but during this contract was adapted to take advantage of the many more colors that are possible to display using modern personal computers.

The first step in the application of the Loomis-Wood technique is to compile a set of first-guess, self-consistent spectral line positions for the branch or sub-band whose lines are to be identified. For the original Looms-Wood diagram (5), the first-guess line positions had constant spacing. A computer generated map is then constructed in the following way: 1) equal wavenumber segments of the transmittance spectra being studied are selected, 2) each segment is centered on the predicted position of one of the spectral lines in the sub band being analyzed, 3) the segments are then stacked one above the other. If the predicted and observed spectral line positions agree, then the observed spectral line will be centered in the figure forming a straight line. The set of spectral lines forming the sub-band will be on top of one another and form an easily discernible straight line pattern.

If the first-guess transitions are in error, an irregular or curved pattern will be observable. The errors from most calculations follow some sort of pattern. For example, if rotational constants are used to determine the first-guess line positions, and the quadratic dependence on the rotational quantum number J is in error, then a quadratic deviation, as a function of J, from the straight line pattern will be observed. The Loomis-Wood technique makes it easy to discover branch or sub-band spectral

lines, even in dense spectra, and to find and correct differences between observed and predicted line positions, if a reasonable set of initial line positions are available.

The original Looms-Wood diagram (5) was only useful for linear molecules, but it has been possible to extend this technique to asymmetrical molecules like H_2O. This is done by finding sequences of lines where the intensities and positions follow regular patterns. These sequences are not nearly as long as they are for a linear molecule like CO_2, but especially in the case of high temperature spectra, they are clearly visible. The software that was developed to make line assignments and display Looms-Wood diagrams is interactive. A crosshair is moved across the diagram and used to select spectral lines. The software then automatically determines the line centers of the experimental feature and creates a new HITRAN format data file with the updated line parameters.

3.2. Verifying Line Assignments

A procedure was developed to check for self-consistency among the measurements made on different rotation-vibration bands, including bands from different spectral regions. One can think of following paths through the energy level space, where the allowed steps in this path are the observed rotation-vibrational transitions. Starting at a given energy level, the energy of the next level in the path is obtained by simply adding or subtracting (depending on the direction of the path) the energy of the transition. For a closed loop, the ending level is the same as the beginning level and the net energy difference after traversing the path should be zero. If experimentally measured transitions are used, the net energy of the path will not be quite zero, but instead will be a measure of the relative accuracy of the measurements. Calculating the net energy around a closed loop of energy levels is also a very sensitive technique for detecting line assignment errors. If an error in the line assignment has been made, a path that is assumed to form a closed loop will actually not be closed, and the resulting net energy of the path will be much greater than that expected from random experimental fluctuations. Since finding these closed loops manually proved very tedious and time consuming, software was written to automatically generate these closed loops from data files containing the observed molecular transitions.

Finding appropriate sums and differences of observed transitions was also used to predicted the position of molecular transitions that have not yet been identified. The position of a spectral transition can be predicted if a path of connecting observed transitions can be found from the lower state to the upper state. Software was written to automatically make an exhaustive search for all such paths less than a maximum number of steps (typically 6 to 7 transitions). Allowing longer paths would have increased the number of paths that could have been identified, but (due to the accumulation of errors) would have resulted in less accurate predictions of molecular transitions. Paths of length 6 to 7 steps proved to be a good compromise. When several alternate paths were found, a weighted average of the transition frequency predicted by the different paths was

calculated. The weight for each path was taken as the inverse sum of squares of the individual uncertainties of the transitions making up the path.

3.3. Automated Identification

Another identification technique, which was useful for finding the rotation-vibration bands of CO_2, was an automated search of parameter space. It used an iterative least-squares-fits method to search for the set of molecular constants that best fit the experimental data. A difficulty with this approach is that the error function being minimized has a large number of local minimums, making it difficult to find the absolute minimum. A successful approach was to start the search for a minimum from many different positions, finding many local minima but only recording the molecular parameters for the fits that appeared the most promising. In this way, a comprehensive search of the whole parameter space was carried out. The most promising fits were then manually examined in detail using the usual interactive techniques. Performing large number of trial fits consumes a great deal of computer time. However, with the cost of computing hardware coming down, and with the rapid increase in the computational power of the new desktop computers, this technique appears to have a promising future.

4. Molecular Modeling

In addition to the experimental measurements of CO_2 and H_2O, extensive molecular modeling was also performed as part of this contractual effort. Although there are a number of possible modeling techniques, (DND) direct numerical diagonalization (6) has proved the most successful in calculating the extensive sets of energy levels need to support the identification of molecular transitions of high temperature gases. Calculations using the DND technique can also be used to calculate line parameters for molecular transitions that are very difficult to observe experimentally.

Work was performed on CO_2 pentad band parameters in conjunction with researchers from other institutions. This work, for the first time, validates DND band parameter calculations for components of polyads where not all of the bands have been observed. A new CO_2 HITEMP database was generated which incorporates these new measurements and level identifications at the end of each line record. The extra level identifications allows for the vibrational identification of lines whose levels are not defined in HITRAN.

The computer modeling software that is used to fit molecular potential surfaces to the experimental data was upgraded by symmetry-adapting the fitting procedure to utilize the C_{2v} symmetry of triatomic molecules such as H_2O, CO_2, and O_3. This makes rovibrational level identification easier and more certain and reduces computer resource requirements. The updated software was then used to find a stable quartic potential

surface for water. A new hot water database was also generated. This database achieves better convergence for high combined vibrational and rotational states.

An H_2S spectroscopic database has been generated using molecular surfaces obtained from recent work of Kozin and Jensen (7) (potential surface) and re-adjustment of the dipole-moment surface published by Carter et al. (8). Comparisons with the new HITRAN database for H_2S show that there are line identification problems and possibly line intensity problems with the HITRAN 92 database.

5. CO_2 Measurements

The details of the CO_2 measurement program are described in journal articles included in the Appendix and will not be duplicated here.

6. H_2O Measurements

A 20 torr sample of natural isotopic abundance H_2O was heated to 1000K in the high temperature absorption cell and observed with the high resolution interferometer spectrometer. A background spectrum was first collected with the sample cell evacuated. The background spectrum was collected at the same resolution as the sample spectrum. For phase correction, a short two-sided spectrum of 123 cm^{-1} resolution was collected. The sample spectrum was collected over a 12-hour period, of which approximately 8 hours was actual data collection time. The remaining time was mirror step and settle-down time. The resulting signal-to-noise ratio (SNR) was better than 100 to 1 in the center of the spectral region studied, near 1050 wavenumbers (see Figure 1). At the high wavenumber end of the spectrum the SNR is lower, as a result of the optical filter cutoff. At the low wavenumber end of the spectrum the system sensitivity decreases as a result of reduced transmission by the numerous zinc selenide windows in the optical path.

6.1. Data Processing

A line-finding computer program was used to determine the spectral line positions in the transmittance spectrum. The program takes into account the spectral line symmetry and the effect of blending by other spectral lines. A total of approximately 1600 spectral line positions were determined from the data shown in Figure 1. The line position uncertainties were determined by the magnitude of the peak absorptance of the spectral line, the width of the line, the signal-to-noise ratio in the region around the spectral line, and the degree to which the line was blended with other lines.

The sample water vapor concentration in the absorption cell was chosen to achieve large absorptance in the weaker spectral lines. This resulted in the stronger lines

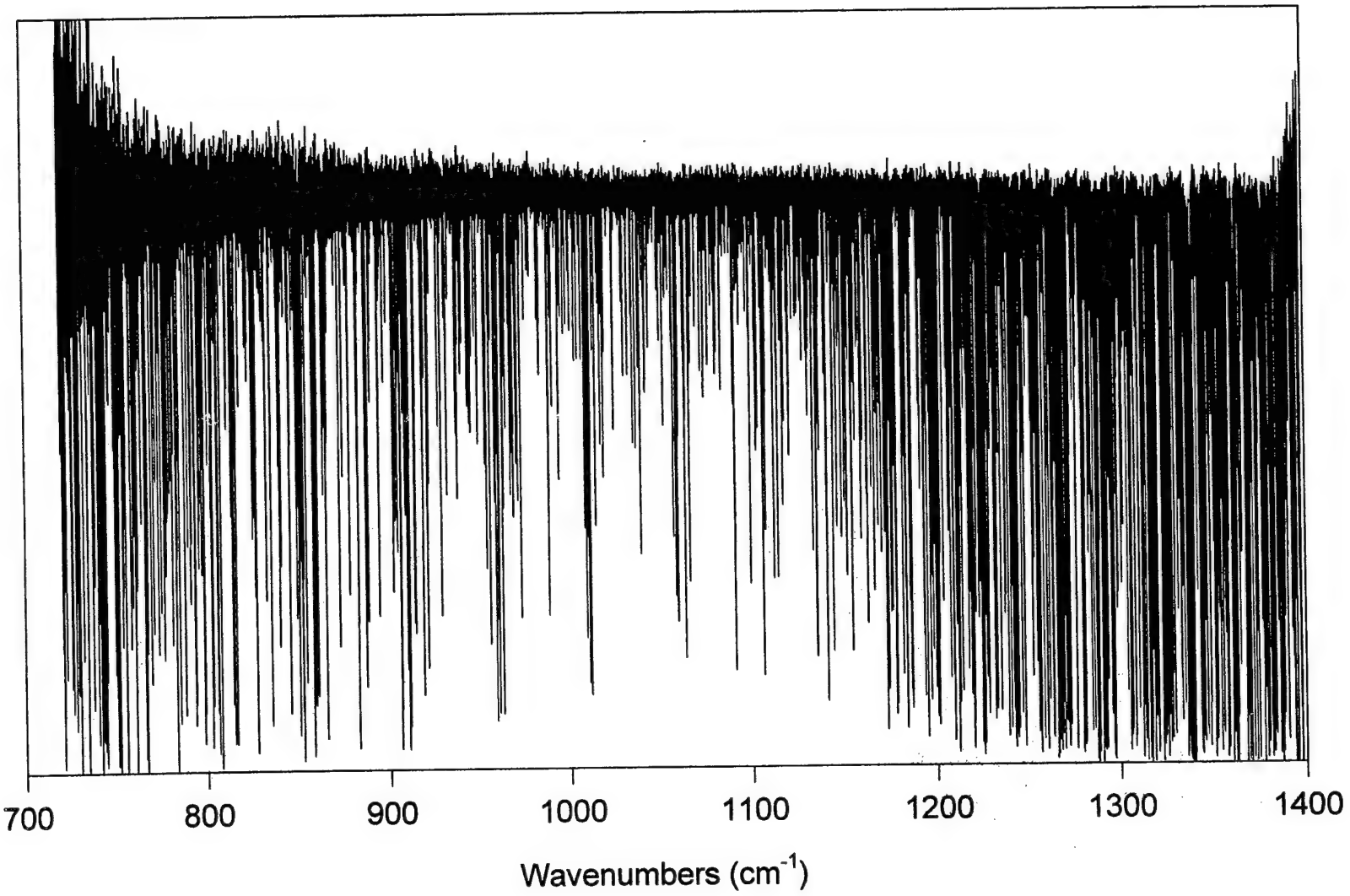

Figure 1. Compressed plot of the measured spectrum of a 20 Torr H_2O sample heated to 1000K.

being saturated near line center. Since these strong lines have been studied previously (9) and are well known, the measured positions of these lines are not reported here. However, these strong lines were used to calibrate the wavelength scale of the spectrometer, because these lines were present in the background spectrum of the absorption cell. Even after being evacuated, the cell contained a small residual amount of water vapor, and the strongest lines were present in the background cell spectra. Forty-nine background spectral lines, spread across the observed spectral region from 1225 to 1398 cm^{-1} were used for calibration. The standard deviation of the calibration residuals was $3.9x10^{-4}$ cm^{-1}.

The 1600 measured spectral line positions, were combined with observed transitions from other studies, to form a self-consistent set of transitions which could then be used to determine energy levels and transition identifications. The additional transitions included 162 lines calculated from energy levels reported by Toth (10), and 70 microwave spectral lines measured by Pearson et al. (11). The most difficult step in the data processing was correctly identifying the molecular transitions. Of the 1600 measured spectral line positions, a total of 921 ro-vibrational transition identifications were made with certainty. Many additional transition assignments were made, but these could not be confirmed by the methods outlined below.

A number of different techniques were used to make the transition assignments. For very well know H_2O spectral lines it was possible to unambiguously pick the observed transition closest to the position given in the HITRAN data base (9). But for most of the transitions discernible at high temperatures, more sophisticated techniques were required to unambiguously make the identification. An enhanced Loomis-Wood diagram-like technique, combined with DND results (6) proved extremely valuable in making line assignments.

An automated combination difference approach also proved very useful in verifying correct identifications. The technique was also used to identify additional transitions, once a number of the transitions had been successfully identified. The identification was made in an iterative manner. First, a number of lines were identified. Knowledge of the energy levels derived from these identified lines was used to identify additional lines. The process could then be repeated, allowing the further identification of additional lines.

In past studies of carbon dioxide (4, 12), an enhanced version of the original Loomis-Wood diagram technique (5) was used to identify spectral lines in P, Q, and R branches. At high temperatures the spectrum is crowded with many more spectral lines than at room temperature. The Loomis-Wood technique was very useful in identifying spectral lines of a particular band. It has been possible to extend our modified Loomis-Wood diagram technique to the asymmetrical molecule H_2O. The rotational energy states of H_2O are generally enumerated using the quantum number J for the total angular momentum, and K_a and K_c for components of the angular momentum. In order

for the Looms-Wood diagram technique to be effective, sequences of transitions need to be calculated where the line intensities and positions follow regular patterns. The H_2O sub-bands for a given K_a and constant ΔK_a and ΔJ are examples of these sequences. These sequences are not as long as for a linear molecule like CO_2, but especially in the case of high temperature spectra, they are clearly discernible using the Loomis-Wood technique.

The first-guess, self-consistent spectral line positions needed to create a Loomis-Wood diagrams were obtained either from the HITRAN data base (9), or from an application of the direct numerical diagonalization (DND) calculation technique. The DND calculation for H_2O used essentially the same method (6) as was previously used for CO_2. A 47-parameter potential surface, with up to hextic powers in internal coordinates, was generated with a nonlinear least-squares fit to observed data. The residuals of the fit result in an RMS of 0.03 cm^{-1} for the 263 rovibrational energy levels used as input to the calculation.

6.2. Results

From the observed H_2O molecular transitions, a set of self-consistent transitions was calculated using an iterative approach. In addition to using the observed transitions from this work, selected transitions from a room temperature H_2O measurement by Toth (10) and microwave transitions from Pearson (11) were also included. Combining information from different regions of the electromagnetic spectrum improves the accuracy of the calculation. This happens not only because of the increase in accuracy that additional measurements provide, but also by reducing the correlation in the calculation. For each iteration, the position of a transition was calculated from a weighted average of the positions predicted using combination differences of the other transitions. In the next iteration, the transitions were replaced with the positions calculated in the preceding iteration. This process was iterated until convergence was achieved.

A total of 921 lines were identified in the experimental spectrum. Actually, considerably more than the 921 transitions reported were observed, but it was only these lines that could be verified using the combination difference technique explained earlier. Positional uncertainties were estimated from the quantity of random noise in the experimental spectral, line strengths, and blending of unresolved lines. The amount of line blending from unresolved lines was estimated from asymmetry in the line profiles and inconsistent line width for a given intensity.

When the H_2O line positions determined in this work were compared with the line positions on the HITRAN 92 database (9), discrepancies of up to 0.8 cm^{-1} were found (Figure 2) for some transitions. These large discrepancies probably arose from the inclusion of data from misidentified H_2O lines on the HITRAN 92 database. In the bottom panel of Figure 2, the vertical scale has been expanded by a factor of 10. It can

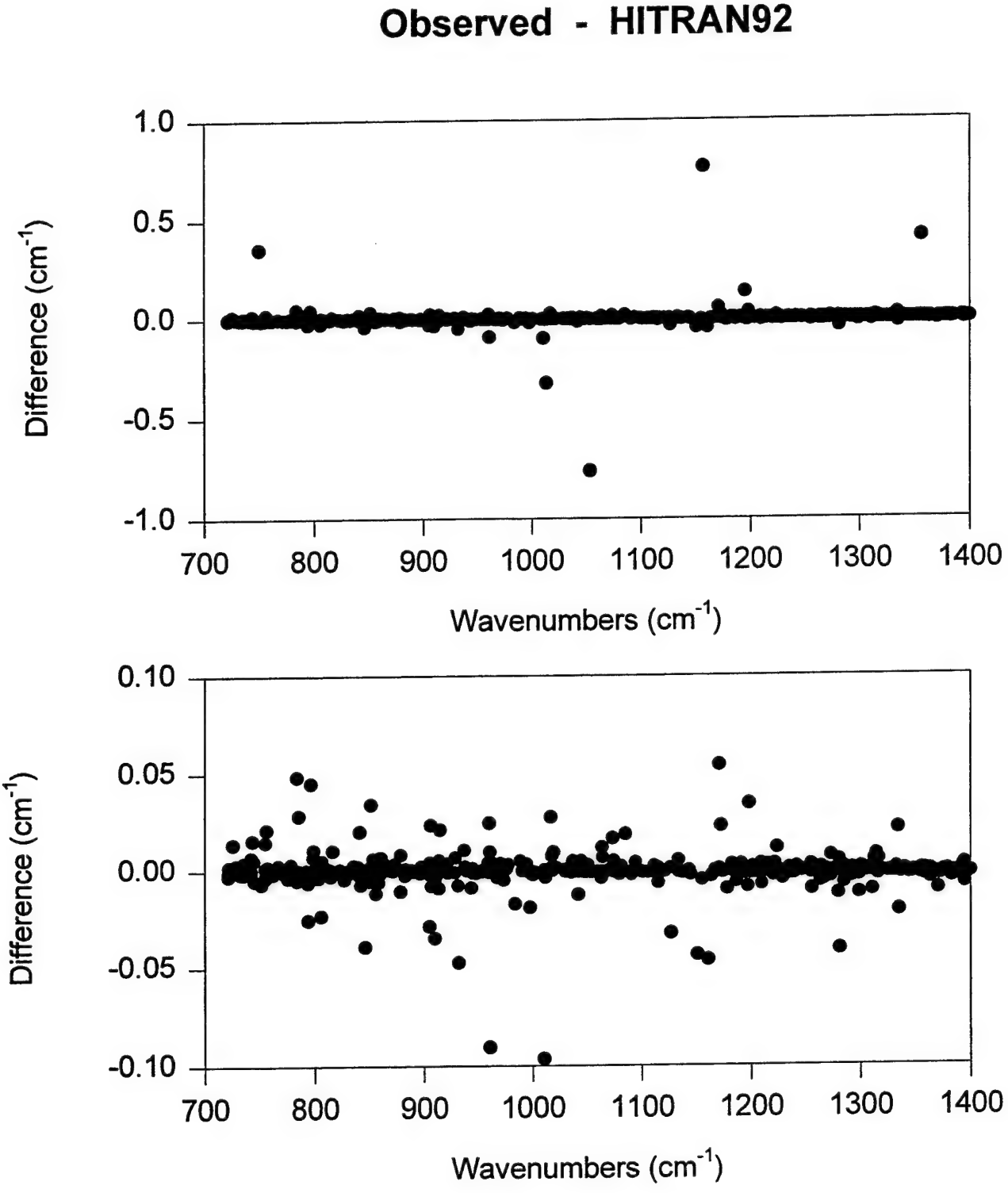

Figure 2. Comparison of observed H_2O line positions with line positions from the HITRAN 92 database. The vertical scale has been expanded by a factor of 10 in the bottom panel.

be seen that there are a number of additional lines where the difference is smaller than 0.1 cm^{-1}, but still large compared to the experimental uncertainty of about 0.0004 cm^{-1}. The HITRAN database is an evolving source of data on atmospheric molecules. Hence, H_2O lines from the present work have been incorporated into the HITRAN 96 database.

7. Scientific Papers

Papers describing the research performed under the present contract are listed below. The full text of the articles, that have been published in scientific journals and in the proceedings of scientific meetings, is included in the appendix of this reports. Other papers presented at international meeting are also listed.

Journal and Proceedings Articles.

M.P. Esplin and M.L. Hoke, "High Temperature, High Resolution Line Position Measurements of $^{12}C^{16}O_2$ in the 580 to 940 cm^{-1} Region," *J. Quant. Spectrosc. Radiat. Transfer* Vol. **48**, 573 (1992).

R.A. Parker, M.P. Esplin, R.B. Wattson, M.L. Hoke, L.S. Rothman, and W.A.M. Blumberg, "High Temperature Absorption Measurements and Modeling of CO_2 for the 12 Micron Window Region," *J. Quant. Spectrosc. Radiat. Transfer* Vol. **48**, 591 (1992).

Mark P. Esplin and Michael Hoke, "Carbon Dioxide Line Positions in the 780 to 940 Wavenumber Region," 8th International Conference on Fourier Transform Spectroscopy, Lübeck-Travemünde, Germany, September 1-6, (1991).

Mark P. Esplin and Michael Hoke, "Band Centers and Line Positions of Hot Bands of $^{13}C^{16}O_2$ and $^{16}O^{13}C^{18}O$ in the 15 Micron Region," High Resolution Fourier Transform Spectroscopy Topical Meeting, Boulder, Colorado, August 27-29, (1992).

Mark P. Esplin and Michael L. Hoke, "High Temperatures Isotopically Enriched CO_2 Line Positions in the 740 to 1060 cm^{-1} Region," 9th International Conference on Fourier Transform Spectroscopy, the University of Calgary, Calgary, Alberta, Canada, August 23-27, (1993).

L.P. Giver, C. Chackerian, Jr., M.N. Spencer, L.R. Brown, and R.B. Wattson, "The Rovibrational Intensities of the $(40^01) \leftarrow (00^00)$ Pentad of $^{12}C^{16}O_2$ between 7284 and 7921 cm^{-1}" *J. Mol. Spec.*, Vol **175**, 104 (1996).

Papers Presented at International Meetings.

Mark P. Esplin and Michael Hoke, "Line Positions of CO_2 in the 580 to 940 cm^{-1} Region at Elevated Temperatures," Forty-Fifth Symposium on Molecular Spectroscopy, The Ohio State University, Columbus, Ohio, (1990).

Mark P. Esplin and Michael Hoke, "Spectra of ^{13}C Enriched CO_2 at Elevated Temperatures in the 15 μm Region," Forty-Sixth Symposium on Molecular Spectroscopy, The Ohio State University, Columbus, Ohio, (1991).

Mark P. Esplin and Michael Hoke, "Line Positions of $^{13}C^{16}O_2$ and$^{13}C^{16}O^{18}O$ Bands in the 580 to 1070 cm^{-1} Region at Elevated Temperatures," Forty-Seventh Symposium on Molecular Spectroscopy, The Ohio State University, Columbus, Ohio, (1992).

M.P. Esplin and M.L. Hoke, "High-Temperature $^{13}C^{16}O_2$ and $^{13}C^{16}O^{18}O$ Line Positions in the 580 to 1060 cm^{-1} Region," Third HITRAN Spectroscopic Database Conference, Geophysics Directorate, Hanscom AFB, MA, June 10-11, (1993).

M.P. Esplin, R.B. Wattson, and M.L. Hoke, "Application of the Loomis-wood Diagram Technique to the High Temperature Spectrum of H_2O," Forty-Eighth Symposium on Molecular Spectroscopy, The Ohio State University, Columbus, Ohio, (1993).

Mark P. Esplin, Richard B. Wattson, Michael L. Hoke, and Laurence S. Rothman "High Temperature Spectrum of H_2O in the 1000 to 1400 cm^{-1} Region," Thirteenth Colloquium on High Resolution Molecular Spectroscopy, Riccione, Italy, Sept 13-17, (1993).

M.P. Esplin, R.B. Wattson, and M.L. Hoke, "H_2O Line Position Measurements at 1000K," Forty-Ninth Symposium on Molecular Spectroscopy, The Ohio State University, Columbus, Ohio, (1994).

References

1. Hajime Sakai, "High Resolving Power Fourier Spectroscopy," *Spectrometric Techniques* **1**, G. Vanasse, ed. Academic Press, New York, NY (1977).

2. Mark P. Esplin, Hajime Sakai, Laurence S. Rothman, George A. Vanasse, William M. Barowy, Ronald J. Huppi, "Carbon Dioxide Line Positions in the 2.8 and 4.3 Micron Regions at 800 Kelvin," ADA173808 (1986).

3. W.S. Dalton and H. Sakai, "Absorption Cell for the Infrared Spectroscopy of Heated Gas," *Appl. Opt.* **19**, 2413 (1980).

4. Mark P. Esplin and Michael Hoke, "Hot Bands of Carbon Dioxide in the 15 Micron Region," High Resolution Fourier Transform Spectroscopy 1989 Technical Digest Series **6**, 27 (1989).

5. F.W. Loomis and R.W. Wood, "The Rotational Structure of the Blue-Green Bands of Na_2," *Phys. Rev.* **32**, 223 (1928).

6. R.B. Wattson and L.S. Rothman, "A Determination of Vibrational Energy Levels and Parallel Band Intensities of $^{12}C^{16}O_2$ by Direct Numerical Diagonalization," *J. Molec. Spectrosc.* **119**, 83 (1986); and R.B. Wattson and L.S. Rothman, "Direct Numerical Diagonalization: Wave of the Future," *J. Quant. Spectrosc. Radiat. Transfer* **48**, 763 (1992).

7. I. N. Kozin and P. Jensen, "Fourfold Clusters of Rovibrational Energy Levels for H_2S Studied with a Potential Energy Surface Derived From Experiment," *J. Molec. Spectrosc.* **163**, 483 (1994).

8. S. Carter, P. Rosmus, N.C. Handy, S. Miller, J. Tennyson, B.T. Sutcliffe, "Benchmark Calculations of First Principles Rotational and Ro-Vibrational Line Strengths," *Computer Phys. Comms.* **55**, 71 (1989).

9. L.S. Rothman, R.R. Gamache, R.H. Tipping, C.P. Rinsland, M.A.H. Smith, D. Chris Benner, V. Malathy Devi, J.-M. Flaud, C. Camy-Peyret, A. Perrin, A. Goldman, S.T. Massie, L.R. Brown, and R.A. Toth, "The HITRAN Molecular Database: Editions of 1991 and 1992 *J. Quant. Spectrosc. Radiat. Transfer* **48**, 469 (1992).

10. Robert A. Toth, "ν_2 Band of $H_2{}^{16}O$: Line Strengths and Transition Frequencies," *J. Opt. Soc. Am. B*, **8**, 2236 (1991).

11. J.C. Pearson, Todd Anderson, Eric Herbst, Frank C. De Lucia, and Paul Helminger, "Millimeter- and Submillimeter-Wave Spectrum of Highly Excited States of Water," *The Astrophysical Journal* **379**, L41 (1991).

12. M.P. Esplin and M.L. Hoke, "High Temperature, High Resolution Line Position Measurements of $^{12}C^{16}O_2$ in the 580 to 940 cm^{-1} Region," *J. Quant. Spectrosc. Radiat. Transfer* **48**, 573 (1992).

Appendix A

High Temperature, High Resolution Line Position Measurements of $^{12}C^{16}O_2$ in the 580 to 940 cm^{-1} Region

J. Quant. Spectrosc. Radiat. Transfer Vol. 48, No. 5/6, pp. 573–580, 1992
Printed in Great Britain.

0022-4073/92 $5.00 + 0.00

HIGH TEMPERATURE, HIGH RESOLUTION LINE POSITION MEASUREMENTS OF $^{12}C^{16}O_2$ IN THE 580 TO 940 cm^{-1} REGION

M. P. ESPLIN† and M. L. HOKE‡

†Utah State University, Stewart Radiance Laboratory, 139 The Great Road, Bedford, MA 01731 and
‡Phillips Laboratory, Geophysics Directorate, Hanscom Air Force Base, MA 01731, U.S.A.

(Received 10 December 1991; received for publication 16 June 1992)

Abstract—More than 6500 *P*, *Q* and *R* branch spectral lines in the region 580–940 cm^{-1} have been identified and assigned to 43 vibration–rotation bands of the principal isotope of carbon dioxide, $^{12}C^{16}O_2$. The position of each line was measured and an uncertainty in the position of each line was estimated. The interferometric data used in this study were obtained from naturally occurring samples of carbon dioxide heated to 800 K, to yield data on high quantum-number rotational, vibrational and vibrational angular momentum states. Measurements were made for three different sample pressures: 5, 15 and 40 torr. Measurements at 15 and 40 torr permitted the observation of weak, high quantum-number vibrational transitions normally not observed at room temperature and high-quantum-number rotational transitions within the vibrational transitions. A maximum unapodized instrumental resolution of 0.0044 cm^{-1} was used. A weighted linear least-squares procedure was applied to the spectral lines of each vibrational transition to estimate rotational–vibrational molecular constants G_v, B_v, D_v and H_v which are reported here.

INTRODUCTION

The objective of the current study is the determination of spectral line positions of carbon dioxide. The goal is to collect spectral data with the largest possible number of observed spectral lines corresponding to high quantum-number rotational, vibrational and vibrational angular momentum transitions. The set of assigned and measured line positions resulting from the data analyses may then be combined with data from other sources and used with available theoretical and computational methods[1] in the determination of a much larger set of line positions for inclusion in the HITRAN[2-4] and HITEMP[5-7] data bases. To study spectral lines corresponding to high quantum numbers, the gas sample was heated to high temperature. This populates high quantum-number vibrational and rotational energy levels and yields many more bands and more spectral lines in each band than has been available before.[8-12]

EXPERIMENTAL DETAILS

The instrumental arrangement has been discussed in detail elsewhere[13] and will be described only briefly here. The interferometric measurements were made with a step-and-hold Michelson interferometer employing cat's-eye moving and fixed mirrors. The maximum stepping-mirror displacement for this study was 57 cm corresponding to an unapodized resolution of 0.0044 cm^{-1}. The output beams of the cat's-eye mirrors are laterally displaced making both accessible and allowing the use of two detectors. Because the two beams are complementary, the detector signals are differenced to yield the interferometric signal. This arrangement reduces the effect of unwanted external disturbances such as 60 Hz interference, source fluctuations and instrumental drifts. The arrangement provides a very stable system over the 8–15 h period necessary for the collection of a single high-resolution interferogram. Both liquid-helium cooled copper-doped germanium detectors, used for operation in the 15 μm spectral region, are housed in the same dewar to keep their experimental conditions the same. An interference filter was used to limit the spectral range from 580 to 940 cm^{-1}. The interferometer, HeNe reference laser, signal detectors, optical filter wheel as well as all of the infrared and laser transfer optics between the absorption cell and the interferometer are housed in the same chamber which is evacuated during operation.

A 1.75 m stainless-steel gas-sample cell was used in this study. It was housed in a commercial electric furnace which can be heated to at least 800 K. This cell (used in a triple pass Pfund configuration) and furnace have been described previously.[14] For the current set of measurements a single pass through the cell was used. This eliminated optical misalignment problems which result from changes in the cell length with changing temperature, approx. 1 cm from room temperature to 800 K. Only the central windows are at room temperature. However, since only measurements of spectral line positions, and not line strengths or widths, were the object of this study, no attempt was made to characterize these temperature gradients. This instrumental difficulty has been considered in a separate study.[15]

The source chamber contains a Nernst glower, radiation chopper and collimating optics. It is mounted to the absorption cell and evacuated during operation. The hot gas sample not only absorbs but radiates. Locating the chopper in the source chamber in the optical path before the sample cell prevents the emission from the hot gas from being modulated and recorded.

Instrument control, data acquisition as well as interferogram data reduction (including phase correction, apodization and Fast Fourier Transformation) and spectral data analysis (including line finding, line assignment, line position measurement and estimation of molecular constants) are accomplished with personal computers in the laboratory using computer programs written specifically for the purpose.

DATA

Three interferometric data sets, corresponding to gas samples at the same temperature of 800 K and pressures of 5, 15 and 40 torr, were used to obtain the results reported here. Data at sample pressures of 5 and 15 torr were collected at the highest resolution used in the study. But it was necessary to apodize this data to reduce "ringing" in the wings of spectral lines, yielding an approximate resolution of 0.0065 cm^{-1}. At the sample pressure of 40 torr, interferometric data was collected using a mirror displacement of 50 cm. Since ringing in line wings was not as big a problem at this pressure, the interferometric data were transformed unapodized, yielding an approximate resolution of 0.005 cm^{-1}. The data collection procedure was the following: first a low resolution empty-cell background interferogram was collected, then a high-resolution interferogram with gas in the cell and finally a second low-resolution empty-cell background interferogram. If the two empty-cell background spectra were in agreement then they were co-added and ratioed with the high-resolution spectrum to produce a single transmittance spectrum. Multiple data sets collected at the same experimental and gas sample conditions were co-added in the spectral domain as transmittance spectra.

A representative transmittance spectrum is shown in Fig. 1. This spectrum was collected at the highest resolution employed in the study. The lower portion of Fig. 1 is a 1 cm^{-1} segment of the survey spectrum above it, including Q branch lines of one of the many $^{12}C^{16}O_2$ bands which were assigned and analyzed. While only the Q branch lines are indicated in the lower part of Fig. 1, most of the remaining lines have been assigned and measured. However, because of the high density of spectral lines some lines, especially in the dense region around 15 μm, could not be assigned.

The difficulty of assigning spectral lines, in dense spectra, to their proper transitions was not unique to this study and was encountered in earlier studies.[16,17] As a result, an interactive data analysis technique has been developed,[18] based on a modification of the method of Loomis and Wood.[19] The technique has proved very useful in identifying and assigning spectral lines in very dense spectra. To implement the technique however, some preliminary knowledge of the molecular constants for the band to be studied must be available. In this study of spectra of carbon dioxide, that knowledge was available in the HITRAN[3] data base and particularly the HITEMP[5] data base which has been compiled by Selby[5] and Wattson and Rothman[20] from results of theoretical calculations using the technique of Direct Numerical Diagonalization, DND,[6,21] of the molecular Hamiltonian.

RESULTS

Line positions were measured for each of the more than 6500 assigned spectral lines. To aid the determination of spectral line positions, data points were interpolated into the transmittance spectra. This was achieved by zero filling the interferograms by a factor of 16 times their length.

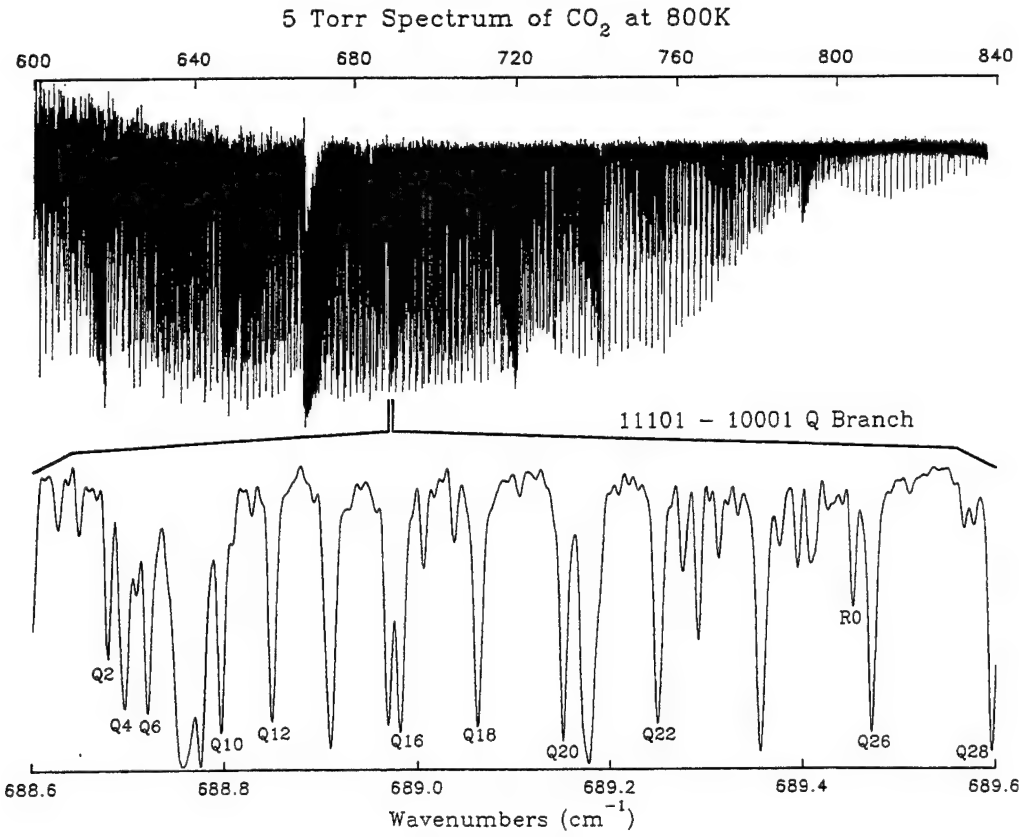

Fig. 1. Transmittance spectrum of 5 torr of a naturally occurring sample of carbon dioxide heated to 800 K. The upper portion of the figure is the complete spectrum; the lower portion is a detail of a 1 cm^{-1} portion showing some of the Q branch lines of the (11101 ← 10001) vibrational transition of $^{12}C^{16}O_2$.

For some rotational–vibrational transitions, line positions were assigned and measured in two or all three transmittance spectra which were analyzed. In those cases the individual position measurements were averaged to yield a single final value: that value was a weighted average of the three separate measurements, weighted with the respective position uncertainties. The corresponding final value of the position uncertainty was computed as the r.m.s. value of the separate estimates of the uncertainty. The estimated uncertainty of individual line positions was based on an estimate of the random noise in the spectrum, the width and the strength of the line. If the line was blended, then the width and a measure of the asymmetry of the blended spectral feature also affected the estimate of the uncertainty. Besides their inherent value, the estimated position uncertainties were used as weighting factors in the least squares determination of molecular constants.

Spectral line positions were calibrated using P, Q and R branch lines, for (J) less than 60, of the (02201←01101) transition. Reference line positions were taken from the HITRAN data base. They are based on the experimental measurements of Jolma et al.[10] For the spectrum shown in Fig. 1 the average line position difference was found to be $-0.00038\ cm^{-1}$. Assigning this value to the band center frequency of this transition, $667.7517\ cm^{-1}$, and assuming a linear correction passing through zero at zero wavenumbers, a linear correction was made to all of the measured line positions.

The measured line positions were assigned to the 43 vibrational transitions indicated in the energy level diagram, Fig. 2. The energy levels are designated by the notation (v_1, v_2, l, v_3, r) in which (v) indicates a vibrational quantum number, (l) the vibrational angular-momentum quantum

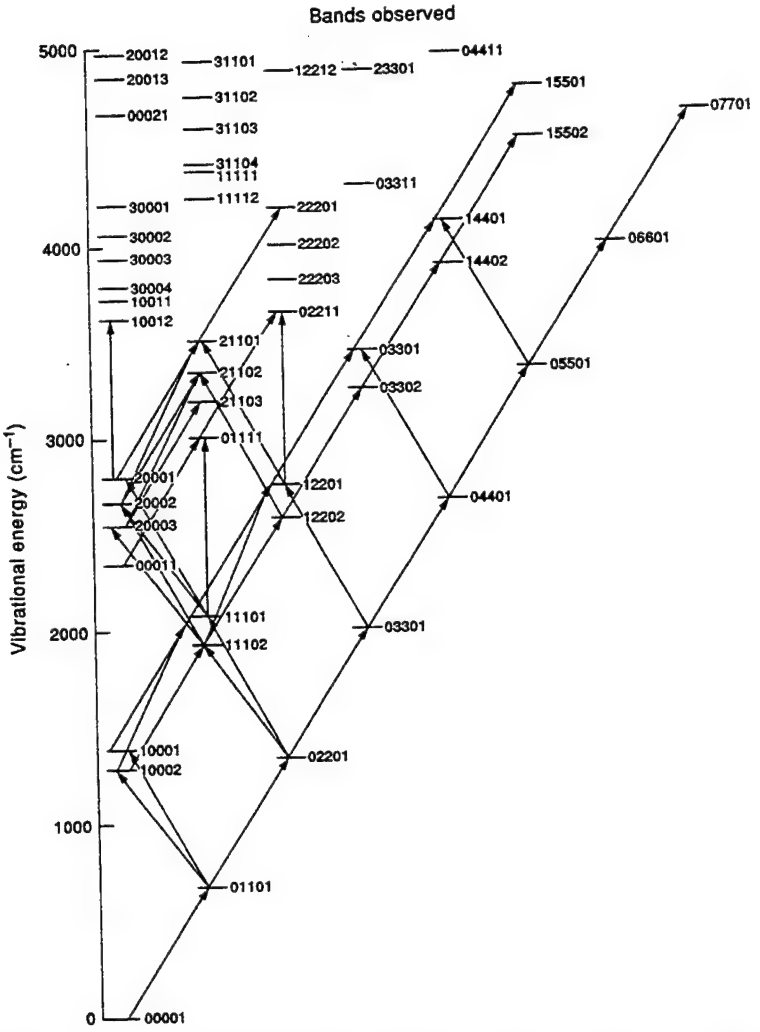

Fig. 2. Energy level diagram indicating vibrational transitions analyzed in this study. Each energy level is designated by the notation (v_1, v_2, l, v_3, r) in which (v) indicates a vibrational quantum number, (l) the vibrational angular momentum quantum numbe and (r) the sequence number of a Fermi resonance group.

number and (r) the sequence number of a Fermi resonance group.[22] The expression for the energy levels used in the least squares determination of the molecular constants (G_v, B_v, D_v, H_v) was the following:

$$E_v(J) = G_v + B_v[J(J+1)] - D_v[J(J+1)]^2 + H_v[J(J+1)]^3 \quad (1)$$

where the subscript (v) indicates the vibrational state dependence and (J) is the rotational angular momentum quantum number. States for which ($l > 0$) exhibit l-type doubling and two sets of energy levels, labeled (e) and (f), result for these states. In the process of least squares fitting spectral lines positions, for bands with l-type doubling, the following approximate relations among molecular constants[3,23] were assumed and employed as constraints for both upper and lower states: if $l = 1$ then it is approximately correct to require that $G_e = G_f$; if $l = 2$ then in addition $B_e = B_f$; further, if $l = 3$ then in addition $D_e = D_f$; and finally if $l = 4$, then $H_e = H_f$. The application of these constraints may be seen in Table 1. For example, the transition (14402←13302), centered at 657.6911 cm^{-1}, has for the upper state all pairs of (e) and (f) rotational–vibrational constants constrained to be equal since $l = 4$, but for the lower state has $H_e \neq H_f$, since $l = 3$.

Approximately 900 of the 6500 measured line positions had large position uncertainties, usually because of line blending. As a result, these lines had very small weights and as a consequence had very little effect in the determination of molecular constants. For some bands there was an insufficient number of spectral lines to estimate H' or H''. This was determined quantitatively by comparing the least-squares fit with and without H' and H'' included, and by considering the magnitude of the standard deviation of H' and H'' as estimated by the least-squares algorithm.

Table 1. Rotational–vibrational constants (cm^{-1}).

Transition		Band Center	B'	D'x10^7	H'x10^{13}	B"	D"x10^7	H"x10^{13}	Range of Measurement			RMS Error x10^4
20002	11101e	594.2862	.38952038	3.90141		.39034317	3.94543		P(0)		R(49)	4
	11101f					.39128975	3.75775			Q(42)		
11102e	02201e	597.3382	.39075045	1.51491	1.2762	.39167173	1.39338	-3.4673	P(20)	Q(64)	R(68)	4
11102f	02201f		.39169510	1.57767	.1922	.39167173	1.39908	.2643	P(21)	Q(75)	R(67)	
20003	11102e	615.8971	.39110392	1.76174	-11.0714	.39074060	1.44822	-15.5401	P(45)		R(77)	4
	11102f					.39168504	1.51260	-14.9594		Q(74)		
10002	01101e	618.0283	.39048215	1.57126	3.6409	.39063916	1.35498	1.9061	P(47)		R(83)	4
	01101f					.39125457	1.36073	1.5600		Q(102)		
21103e	20003	633.0965	.39101576	1.59693	-4.4813	.39110177	1.76861	-2.0946	P(60)	Q(72)	R(84)	4
21103f			.39234415	1.71558	-5.6512							
11102e	10002	647.0621	.39074843	1.50989	2.6946	.39048573	1.58681	3.9414	P(82)	Q(98)	R(96)	3
11102f			.39169388	1.58043	3.0562							
12202e	11102e	652.5520	.39194285	1.39067	-7.7153	.39074426	1.48459	.0110	P(69)	Q(77)	R(81)	4
12202f	11102f		.39194285	1.52498	.4271	.39168975	1.55475	.2831	P(68)	Q(86)	R(76)	
01111e	00011	654.8692	.38759109	1.34134		.38713955	1.32292		P(63)	Q(79)	R(77)	4
01111f			.38818864	1.35034								
02211e	01111e	655.2611	.38862828	1.28985	-13.5147	.38758857	1.30372	-4.9906	P(46)	Q(50)	R(62)	5
02211f	01111f		.38862828	1.30096	-10.6679	.38818574	1.30074	-8.4453	P(0)	Q(63)	R(61)	
13302e	12202e	655.6007	.39266100	1.50454	-1.3724	.39194618	1.40487	-6.3414	P(58)	Q(74)	R(74)	4
13302f	12202f		.39266100	1.50454	-.4041	.39194618	1.53834	1.6257	P(53)	Q(75)	R(71)	
14402e	13302e	657.6911	.39336868	1.57866	8.4642	.39266449	1.55848	8.0177	P(39)	Q(59)	R(53)	4
14402f	13302f		.39336868	1.57866	8.4642	.39266449	1.55848	9.3049	P(42)	Q(60)	R(64)	
15502	14402	659.2812	.39402451	1.44331		.39332854	1.41409		P(38)	Q(53)	R(50)	6
01101e	00001	667.3820	.39063749	1.34760	-.3020	.39021820	1.32899	-.2952	P(100)	Q(102)	R(118)	6
01101f			.39125348	1.35623	-.2236							
02201e	01101e	667.7517	.39166733	1.37805	-3.2460	.39063942	1.35570	.3961	P(85)	Q(107)	R(109)	3
02201f	01101f		.39166733	1.38324	.4566	.39125528	1.36398	.4642	P(92)	Q(92)	R(100)	
03301e	02201e	668.1143	.39237963	1.40271	-1.4051	.39166770	1.37632	-3.5065	P(88)	Q(92)	R(98)	3
03301f	02201f		.39237963	1.40271	-1.0203	.39166770	1.38164	.2027	P(77)	Q(89)	R(97)	
21102e	20002	668.2117	.39003423	1.37973	4.0871	.38955873	1.34198	6.7684	P(60)	Q(76)	R(66)	4
21102f			.39116906	1.36800	2.5075							
04401e	03301e	668.4683	.39308333	1.42338	-1.2637	.39237956	1.39955	-1.6632	P(67)	Q(91)	R(91)	3
04401f	03301f		.39308333	1.42338	-1.2637	.39237956	1.39955	-1.2682	P(72)	Q(90)	R(92)	
05501	04401	668.8133	.39378173	1.46006		.39308650	1.43753		P(61)	Q(82)	R(78)	4
06601	05501	669.1490	.39445068	1.44365		.39376251	1.41551		P(54)	Q(56)	R(62)	6
07701	06601	669.4789	.39504365	.53987		.39436883	.46312		P(36)	Q(0)	R(51)	8
15501	14401	679.0954	.39354118	1.43111		.39289125	1.39829		P(0)	Q(50)	R(56)	9
14401e	13301e	680.0528	.39288436	1.44956	6.8164	.39222547	1.42291	4.9304	P(49)	Q(55)	R(61)	5
14401f	13301f		.39288436	1.44956	6.8164	.39222547	1.42291	7.3657	P(30)	Q(62)	R(70)	
13301e	12201e	681.4905	.39222253	1.39456	.4304	.39155483	1.44679	-2.6525	P(60)	Q(74)	R(80)	3
13301f	12201f		.39222253	1.39456	2.1460	.39155483	1.31285	4.4836	P(51)	Q(77)	R(83)	
12201e	11101e	683.8688	.39154667	1.40730	-8.2658	.39040845	1.24797	-1.4756	P(67)	Q(91)	R(89)	4
12201f	11101f		.39154667	1.27136	-1.4948	.39133283	1.19999	-2.1340	P(64)	Q(84)	R(82)	
11101e	10001	688.6717	.39041007	1.26330	1.4098	.39018913	1.15296	2.2521	P(86)	Q(98)	R(100)	3
11101f			.39133420	1.21497	.8864							
22201e	21101e	696.6889	.39158510	1.58605	-12.8905	.39037834	1.16217	1.3007	P(33)	Q(59)	R(59)	5
22201f	21101f		.39158510	1.17285	-1.0853	.39170651	1.06891	-2.5659	P(30)	Q(52)	R(58)	
21101e	20001	703.5363	.39037627	1.09817	-11.9045	.39059403	.88971	-12.1256	P(62)	Q(82)	R(90)	4
21101f			.39170327	.99802	-16.4455							
20001	11101e	720.2805	.39060187	.94981	1.1959	.39040674	1.23741	-1.9230	P(85)		R(89)	4
	11101f					.39133157	1.19330	-1.9150		Q(94)		
10001	01101e	720.8043	.39018418	1.13590	.8832	.39063425	1.33935	-.9092	P(87)		R(109)	2
	01101f					.39124998	1.34765	-.8204		Q(106)		

[*continued . . .*]

Table 1—*continued*

Transition		Band Center	B'	D'x10^7	H'x10^{13}	B"	D"x10^7	H"x10^{13}	Range of Measurement			RMS Error x10^4
20002	11102e	738.6731	.38956442	1.35196	5.1490	.39074769	1.49795	.8225	P(71)		R(85)	3
	11102f					.39169274	1.56488	.6246		Q(84)		
21101e	12201e	739.9474	.39038953	1.19459	6.7988	.39155002	1.43548	-2.2209	P(50)	Q(56)	R(84)	4
21101f	12201f		.39171775	1.10214	3.6859	.39155002	1.30024	4.6907	P(63)	Q(75)	R(81)	
11101e	02201e	741.7244	.39040751	1.25331	.4825	.39166464	1.36868	-4.1425	P(86)	Q(78)	R(104)	2
11101f	02201f		.39133160	1.20464	-.0919	.39166464	1.37454	-.3431	P(61)	Q(93)	R(101)	
21102e	12202e	754.3333	.39003614	1.37483	.8039	.39194336	1.39154	-8.5872	P(48)	Q(80)	R(70)	4
21102f	12202f		.39117534	1.38462	1.6278	.39194336	1.52651	-.2543	P(61)	Q(81)	R(61)	
12201e	03301e	757.4788	.39154668	1.41102	-6.5531	.39237759	1.39579	-1.7773	P(69)	Q(81)	R(83)	3
12201f	03301f		.39154668	1.27690	.6288	.39237759	1.39579	-1.4634	P(64)	Q(84)	R(80)	
13301e	04401e	770.5010	.39221644	1.37134	-2.0196	.39308332	1.43018	-.5419	P(48)	Q(80)	R(72)	3
13301f	04401f		.39221644	1.37134	-.4280	.39308332	1.43018	-.5419	P(55)	Q(61)	R(73)	
14401	05501	781.7403	.39286713	1.40032		.39376953	1.45164		P(46)	Q(68)	R(64)	5
21102e	20003	790.9890	.39003573	1.35948	-1.4203	.39111015	1.79570	1.7924	P(58)	Q(70)	R(72)	4
21102f			.39117438	1.36341	-1.6540							
11101e	10002	791.4476	.39041013	1.25683	.6090	.39048261	1.56851	1.7648	P(64)	Q(82)	R(86)	3
11101f			.39133425	1.20894	.1439							
12201e	11102e	828.2540	.39155669	1.47737	4.7331	.39075336	1.55961	13.7713	P(51)	Q(61)	R(45)	7
12201f	11102f		.39155669	1.34451	12.5306	.39169830	1.62280	12.8528	P(56)	Q(54)	R(62)	
21101e	20002	829.5295	.39035264	.94544		.38952530	1.09295		P(36)	Q(54)	R(68)	10
21101f			.39168002	.84524								
02211e	12201e	898.5472	.38863918	1.38641	1.4484	.39155000	1.43659	-2.3839	P(64)	Q(30)	R(46)	6
02211f	12201f		.38863918	1.39445	5.4450	.39155000	1.29672	5.3826	P(69)	Q(0)	R(53)	
10011	20001	917.6463	.38709682	1.63747		.39064023	1.43211		P(72)		R(20)	6
01111e	11101e	927.1562	.38758726	1.59061		.39040612	1.48731		P(69)	Q(0)	R(11)	3
01111f	11101f		.38818983	1.32414		.39133264	1.17622		P(76)	Q(0)	R(14)	

If the least-squares fit with H' and H'' included did not reduce the r.m.s. line position error by at least 25%, and if the estimated uncertainty $\langle\sigma_{H'}\rangle$ and $\langle\sigma_{H''}\rangle$ of H' and H'' were comparable to or larger than the magnitude of the estimates $\langle H'\rangle$ or $\langle H''\rangle$, then these parameters were omitted from the fit. Hence, several of the transitions included in Table 1 have no estimates of H' and H''.

The molecular constants given in Table 1 were determined and are reported here for the purpose of reproducing line positions. For that reason the molecular constants were treated as fitting parameters in the least-squares analyses and not as physical parameters. As a consequence the spectral lines of each vibrational transition were least-squares fit independently of spectral lines of other vibrational transitions, even though some of these transitions shared common states. And for the same reason, the parameter standard deviations estimated by the least squares algorithm are not reported in Table 1. Instead, the number of significant figures included in the table was determined by the precision to which the molecular constants may be used to predict line positions. The precision chosen was 0.0001 cm^{-1} corresponding to a rotational quantum number (J) equal to 100. This criterion was uniformly applied to all of the measured bands and accounts for the fact that the number of significant figures in the table is the same for all of the B's, and similarly for D's and H's. However, the molecular constants in Table 1 should not be used to extrapolate the calculation of line positions beyond the measurement range which is also given in Table 1.

The analysis of the $^{12}C^{16}O_2$ fundamental (01101←00001) is a special case in this study. To identify, assign and analyze spectral lines of weaker bands, the amount of CO_2 gas used in the cell was large enough that the line centers of the low (J) lines of the fundamental (below J of approx. 60) are saturated and their line positions are not well determined. However, the line centers of the high (J) lines (above J of 60) were not saturated and their positions could be well determined. The molecular constants in Table 1 reflect this fact. For example, the band center is not, and could not be, well determined.

Several of the transitions shown in Fig. 1 have not been analyzed previously and the line positions and molecular constants (for those bands) measured in this study are new. This includes the following transitions: (05501 ← 04401), (06601 ← 05501), (07701 ← 06601) as well as (15502 ← 14402) and (15501 ← 14401). Lines of the transition (08801 ← 07701) were found to be present in the figures generated with the modified Loomis–Wood technique described above, but

these lines were very weak and the number of lines was insufficient to perform an analysis. Consequently, no results are included for the (08801 ← 07701) band in Table 1.

Many of the line positions measured in this study have been used to update the HITRAN data base; the latest version is HITRAN92.[24] Figure 3 is an example for the (04401 ← 03301) band. In this figure the solid circles are the line position residuals (observed minus calculated) obtained from this study; the calculated line positions result from using the molecular constants given in Table 1. The r.m.s. value of the line position residuals seen in Fig. 3 (3×10^{-4} cm^{-1}) is also included in Table 1. The solid curves in Fig. 3 are the differences between the line positions calculated from the molecular constants given in Table 1, and the line position values found in the three data bases respective labeled "HITRAN86",[3] "Wattson"[5,20] and "Chedin";[25,26] "Wattson" refers to the DND calculations included in the HITEMP data base. As the curve labeled "HITRAN86" shows, the magnitude of the improvement is significant for rotational quantum numbers greater than +40 and less than −40. It should be noted that the sharp divergence of the "HITRAN86" curve is characteristic of results obtained using polynomial fitting functions, like equation (1), extrapolated outside of the range of the fit. This applies to both the HITRAN86 line positions and the line positions calculated from the molecular constants in Table 1. This emphasizes the importance of not using the molecular constants in the table to extrapolate line positions beyond the range which is also given there. The same divergence of the HITRAN86 line positions relative to the measured positions was found for many other transitions measured in this study. These considerations are more appropriate to the HITEMP database, which includes line parameter data for very high rotational–vibrational quantum-number lines, than they are for the HITRAN database which employs an intensity cutoff criterion[2] which limits the vibrational and rotational quantum-number range of most bands.

The line positions measured in this study and the theoretical values which are found in the HITEMP data base are complementary data sets. Some of the line positions measured in this study will be employed as input data in future DND calculations by Wattson and Rothman; the results will be used to update the HITRAN and HITEMP data bases. Conversely, line positions from the

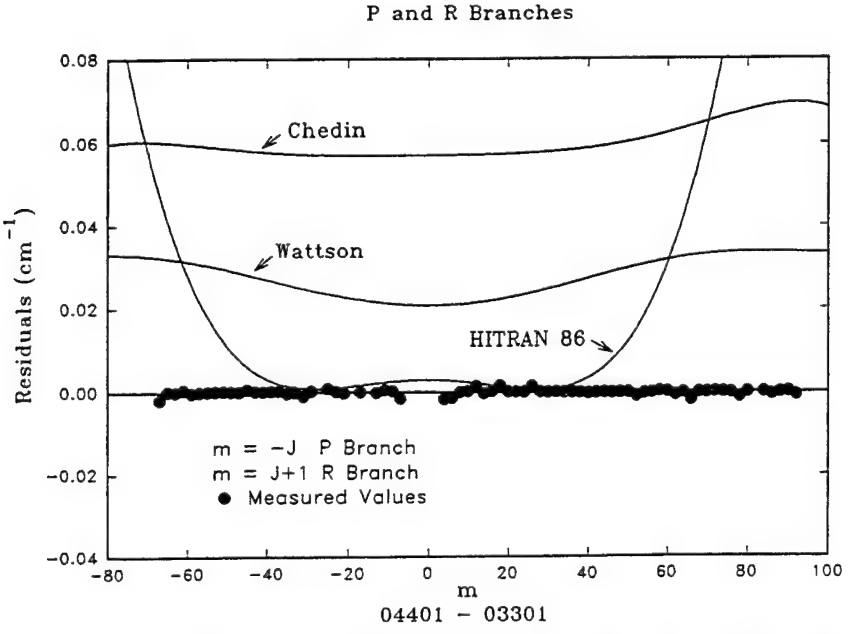

Fig. 3. Line position residuals for the (04401 ← 03301) transition of $^{12}C^{16}O_2$. (●) are the line position residuals (observed minus calculated) obtained from this study; the calculated line positions result from using the molecular constants given in Table 1. (——) are the differences between the calculated line positions from this study and the line position values found in the three data bases; the HITRAN data base, the HITEMP data base and the data base of Chedin.

current version of the HITEMP data base have been very useful in this study for the purpose of identifying and assigning spectral lines, especially those lines corresponding to bands for which there was no data on the HITRAN[3] data base and lines corresponding to high rotational quantum numbers (J). This is illustrated in Fig. 3. For most bands the DND algorithm leaves a small shift compared to the measurements and compared to HITRAN for small values of the rotational quantum number. A general characteristic of the DND calculations is that for high rotational quantum numbers the predicted line positions diverge from the measured values, but much more slowly than do the HITRAN values. In addition, for transitions corresponding to high vibrational quantum numbers, the calculated line positions of Wattson and Rothman[6,20] are in much better agreement with the measured values than the calculated positions of Chedin and Teffo.[25,26]

SUMMARY AND CONCLUSIONS

The positions of 6500 $^{12}C^{16}O_2$ lines in the 15 μm region have been measured. Approximately 325 of these belong to five previously unmeasured vibrational bands. The remaining measurements correspond to previously studied vibrational transitions, but for many of these transitions the measurements of this study are new and extend the range of rotational quantum numbers for which line position measurements are now available. Many of the position measurements of this study will be used to update the HITRAN and HITEMP data bases. An interactive data analysis technique based on the method of Loomis and Wood has proved very useful in assigning spectral lines that otherwise could not have been identified. Molecular constants for 43 rotational–vibrational transitions of $^{12}C^{16}O_2$ have been determined from the measured line positions.

Acknowledgements—The work reported here has been funded by the Air Force Office of Scientific Research as part of PL/GP Task 2310G1. We would like to thank Dr John Johns, for reading the manuscript and for helpful suggestions.

REFERENCES

1. R. L. Hawkins, private communication (1992).
2. L. S. Rothman, R. R. Gamache, A. Goldman, L. R. Brown, R. A. Toth, H. M. Pickett, R. L. Poynter, J.-M. Flaud, C. Camy-Peyret, A. Barbe, N. Husson, C. P. Rinsland, and M. A. H. Smith, *App. Opt.* **26,** 4058 (1987).
3. L. S. Rothman, *Appl Opt.* **25,** 1795 (1986).
4. L. S. Rothman, "Where we are: Commentary on the Current Edition of HITRAN", presented at the *Conf. on Molecular Spectroscopic Databases*, held June 1991 at the Phillips Laboratory, Hanscom AFB, 01731.
5. J. Selby, private communications (1991).
6. R. B. Wattson and L. S. Rothman, *J. Molec. Spectrosc.* **119,** 83 (1986).
7. L. S. Rothman, R. L. Hawkins, R. B. Wattson, and R. R. Gamache, *JSQRT* **48,** 537 (1992).
8. Risto Paso, Jyrki Kauppinen, and Rauno Anttila, *J. Molec. Spectrosc.* **79,** 236 (1980).
9. J. Kauppinen, K. Jolma, and V.-M. Horneman, *Appl. Opt.* **21,** 3332 (1982).
10. K. Jolma, J. Kauppinen, and V.-M. Horneman, *J. Molec. Spectrosc.* **101,** 300 (1983).
11. K. Jolma, *J. Molec. Spectrosc.* **111,** 211 (1985).
12. V. Dana, A. Hamdouni, R. B. Wattson, and L. S. Rothman, *Appl. Opt.* **29,** 2474 (1990).
13. H. Sakai, in *Spectrometric Techniques*, Vol. 1, G. Vanasse, ed. Academic Press, New York, NY (1977).
14. W. S. Dalton and H. Sakai, *Appl. Opt.* **19,** 2413 (1980).
15. R. W. Parker, M. P. Esplin, R. B. Wattson, M. L. Hoke, L. S. Rothman, and W. A. M. Blumberg, *JQSRT* **48,** 591 (1992).
16. M. P. Esplin and L. S. Rothman, *J. Molec. Spectrosc.* **100,** 193 (1983).
17. M. P. Esplin and L. S. Rothman, *J. Molec. Spectrosc.* **116,** 351 (1986).
18. M. P. Esplin and M. L. Hoke, in *High Resolution Fourier Transform Spectroscopy*, Vol. 6, pp 27–30, Optical Society of America, Washington, DC (1989).
19. F. W. Loomis and R. W. Wood, *Phys. Rev.* **32,** 223 (1928).
20. R. B. Wattson, private communications (1991).
21. R. B. Wattson and L. S. Rothman, *JSQRT* **48,** 763 (1992).
22. R. A. McClatchy, W. S. Benedict, S. A. Clough, D. E. Burch, R. F. Calfee, K. Fox, L. S. Rothman, and J. S. Garing, *AFCRL Atmospheric Absorption Line Parameter Compilation*, AFCRL-TR-73-0096, Air Force Cambridge Research Laboratories, Hanscom Air Force Base, Bedford, MA 01731.
23. A. Chedin, *J. Molec. Spectrosc.* **76,** 430 (1979).
24. L. S. Rothman, R. R. Gamache, R. H. Tipping, C. P. Rinsland, M. A. H. Smith, D. Chris Benner, V. Malathy Devi, J. M. Flaud, C. Camy Peyret, A. Perrin, A. Goldman, S. T. Massie, L. R. Brown, and R. A. Toth, *JQSRT* **48,** 469 (1992).
25. A. Chedin and Jean-Luc Teffo, *J. Molec. Spectrosc.* **107,** 333 (1984).
26. A. Chedin, private communication (1984).

Appendix B

High Temperature Absorption Measurements and Modeling of CO_2 for the 12 Micron Window Region

J. Quant. Spectrosc. Radiat. Transfer Vol. 48, No. 5/6, pp. 591–597, 1992
Printed in Great Britain.

0022-4073/92 $5.00 + 0.00

HIGH TEMPERATURE ABSORPTION MEASUREMENTS AND MODELING OF CO_2 FOR THE 12 MICRON WINDOW REGION

R. A. PARKER,† M. P. ESPLIN,‡ R. B. WATTSON,§ M. L. HOKE,¶ L. S. ROTHMAN,¶ and W. A. M. BLUMBERG¶

†Physical Research Inc., 25500 Hawthorne Blvd., Suite 2300, Torrance, CA 90505, ‡Stewart Radiance Laboratory, Utah State University, Bedford, MA 01730, §Visidyne, Inc., 10 Corporate Place, Burlington, MA 01803, and ¶Phillips Laboratory, Geophysics Directorate, Hanscom AFB, MA 01731, U.S.A.

(Received 17 December 1991; received for publication 16 June 1992)

Abstract—High temperature absorption measurements were made for CO_2 gas in Local Thermodynamic Equilibrium (LTE) with a hot cell and high resolution interferometer. The experimental data were compared to band-model and line-by-line model transmittance calculations using line parameters from the HITRAN and HITEMP data bases. The line-by-line calculations using HITEMP were in excellent agreement with experimental measurements, while the model calculations using the HITRAN data underpredicted the absorption by approx. 10%.

INTRODUCTION

For many years, the Department of Defense (DOD) has supported research on sensor design for disturbed atmospheric environments. Because of the computational resources required for such an effort, these computer codes have relied on a band-model characterization of the LTE and non-LTE spectral properties of atmospheric molecules.[1] At normal temperatures the atmosphere has several i.r. transmission windows. At higher temperatures, these windows begin to close primarily because of the i.r. activity of CO_2.

At higher temperatures the absorption spectrum of CO_2 becomes significantly populated with i.r. absorption lines from higher-energy, vibrational states. Experimental efforts to identify and measure the absorption strengths of lines from these highly-excited absorption and emission bands are difficult. Thus, in order to compute more reasonable high-temperature, band-model parameters, currently it is necessary to obtain band-strength and molecular-constant data for highly-excited transitions from quantum mechanical models.

One of the major goals for the present research has been to validate the theoretically derived HITEMP[2] data base for the atmospheric transmission window near 12 μm at high temperature. High-temperature gas samples of carbon dioxide were studied using the high resolution interferometer[3] and high-temperature absorption cell described in Ref. 4. The spectral region covered by these measurements ranged from 600 to 1200 cm^{-1}. For the analysis of the experimental data line-parameter data files were prepared from band-strength and molecular-constant data obtained from the HITEMP and HITRAN[5] data bases. The CO_2 line parameter data in the HITEMP data base was calculated by Wattson and Rothman[2] using a Direct Numerical Diagonalization (DND) technique. Line parameter data for CO_2 was also obtained from the 1986 version of HITRAN.[5] The line lists were input to a line-by-line computer model which calculated transmission of i.r. radiation through the hot cell for the given experimental conditions. Comparisons with the experimental data provided high temperature validation of the DND technique.[6]

EXPERIMENTAL DETAILS

A two-meter optical path difference step and hold "cat's eye" interferometer, high-temperature gas-sample hot cell and Nernst-glower infrared source were used in this study.[4] This interferometer

has been used previously to study two strong absorption regions in CO_2, the 4.3 and the 2.8 μm regions.[7,8] Recently, absorption measurements for the 15 μm region have been performed and analyzed with the aid of theoretical information from the DND model and many new band identifications have been made.[9]

The experimental data described here were collected with a resolution better than 0.1 cm^{-1}. This was sufficient for validation of the DND data base for use with high-temperature, band-model, computer codes. A single-pass, stainless-steel, gas-sample cell[3] 1.75 m in length was housed inside a commercial electric furnace which heated the gas sample to 800 K. The transmission windows on the ends of the cell were outside of the furnace enclosure, and maintained at room temperature. Consequently, there was a temperature gradient in the gas sample.

The experimental data for a pressure of 760 torr and cell length of 175 cm are plotted in Fig. 1. The upper panel is for a cell temperature of 300 K and the lower panel is for a temperature of 800 K. Although the 300 K spectrum was not analyzed for this work, it serves to illustrate the dramatic difference in the appearance of the CO_2 spectrum, that resulted from raising the temperature of the absorption cell from 300 to 800 K. The room temperature spectrum consisted of a single experimental measurement, whereas the 800 K spectrum consisted of 4 experimental measurements coadded together. The integration time for the 800 K measurements was also twice as long as that of the 300 K measurements. Both the 300 and the 800 K spectra were ratioed by the spectrum of the empty cell, to remove the effects of a nonconstant background.

This experimental apparatus was designed specifically for line position measurements, not intensity measurements. However, since only a small portion of the optical path experiences a temperature gradient, the path was treated as isothermal for the relatively low resolution transmission calculations that are presented below. This assumption was checked by performing non-isothermal band-model[10] calculations, based on the results of two-dimensional hydrodynamics code temperature estimates. A more realistic, but computationally intensive, three-dimensional calculation would predict a less rapid drop off in temperature from the central portion of the cell, and a sharper drop near the windows compared to two-dimensional hydrodynamics calculations. Therefore, the two-dimensional calculations give an upper bound on the expected temperature gradient in the hot cell. These calculations indicate that for the experimental conditions of path length (175 cm), pressure (760 torr) and heater temperature (800 K) the absolute-absorption spectrum was affected by less than 1%.

RESULTS

Experimental absorption data for a pressure of 760 torr and a temperature of 800 K were compared to theoretical transmission calculations using the HITRAN data and HITEMP data with band-model and line-by-line model computer codes. A series of comparisons were made between the experimental data and theoretical calculations both of which were convolved with a 5 cm^{-1} FWHM (Full Width at Half Maximum) triangular filter function to average over the rotational line structure.[6]

The theoretical expression of the transmission curve can be reduced to an analytic narrow band statistical model if certain simplifying assumptions are made about the spacing of the lines and the line strength distribution. For this work it is assumed that all lines have Lorentz shape and equal widths, and that the distribution of line strengths is assumed to follow an exponential probability distribution function. The narrow band statistical model[11] calculations using the HITEMP band-strength data and molecular parameters yielded good agreement with the experimental data as shown in Fig. 2. Model calculations using HITRAN data (not shown) predicted about 10% less absorption than the data. This discrepancy is due to the many additional transitions which are treated by the DND model from which HITEMP is compiled, which are not accounted for in the HITRAN compilation. The band-model calculations confirm the appropriateness of applying the HITEMP data-base for the prediction of high temperature absorption and emission characteristics of CO_2. However, band-model calculations rely on simplifying assumptions regarding the distribution of line positions and strengths within a spectral interval.

Line-by-line calculations were also performed. In the line-by-line model, line intensities and positions were computed from the molecular parameters contained in the HITRAN and HITEMP

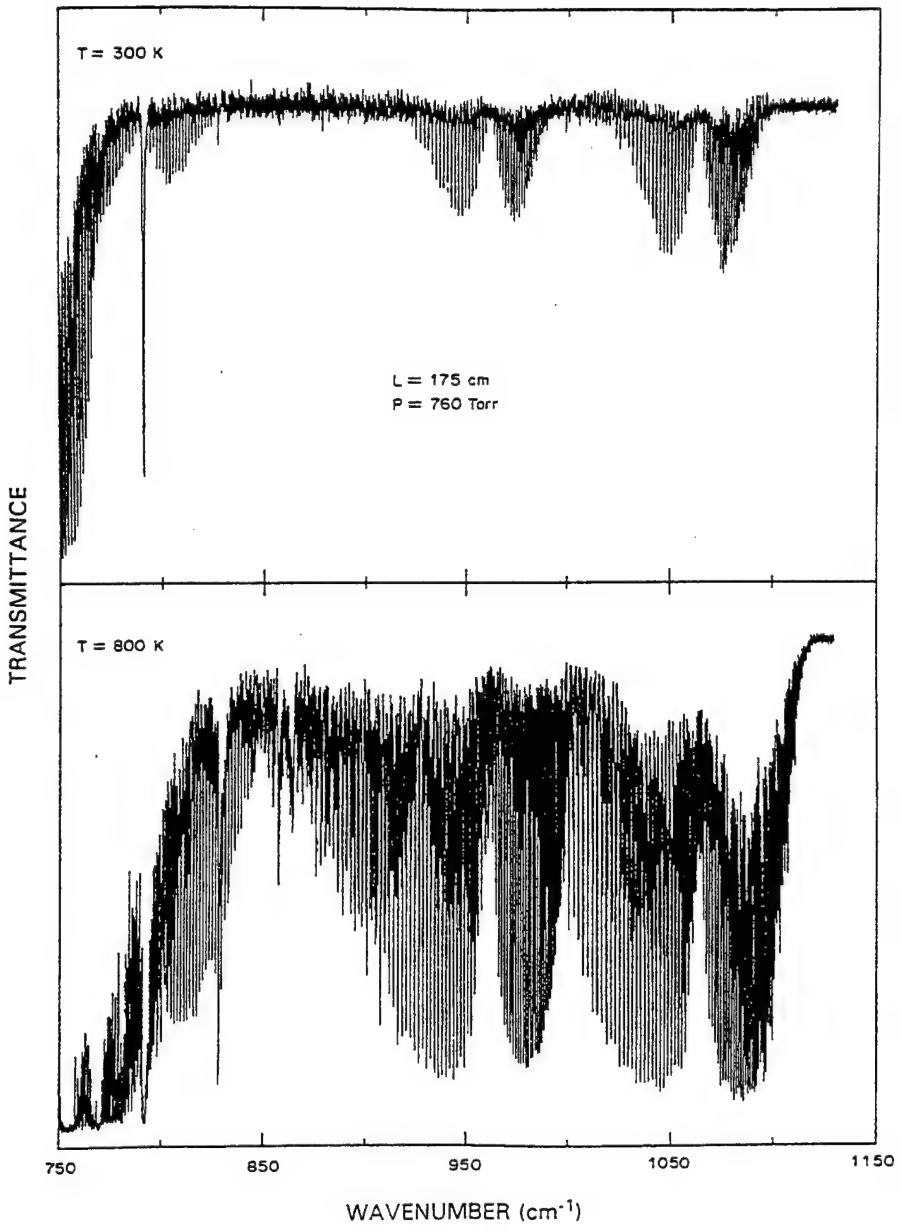

Fig. 1. The experimental data for a pressure of 760 torr and path length of 175 cm are plotted. In the upper panel the spectrum for $T = 300$ K are compared to the $T = 800$ K spectrum in the lower panel.

data bases. For these line-by-line model calculations, an average room-temperature (296 K) self-broadened width for CO_2 lines of 0.07 cm^{-1} was adopted.[12] Assuming a square-root power-law dependence on temperature, an average self-broadened half-width of 0.04 cm^{-1} was calculated for a temperature of 800 K. The line-by-line calculations were performed by generating the line shape for each line with a grid resolution of 0.015 cm^{-1} and carried out to 2.25 cm^{-1} (56 Lorentz line widths) on each side of line center. These line-by-line calculations included lines originating from bands with an integrated band intensity greater than 10^{-8} atm/cm^3. With this cutoff limit and limiting the maximum J to less than 200, more than 20,000 lines were processed using the

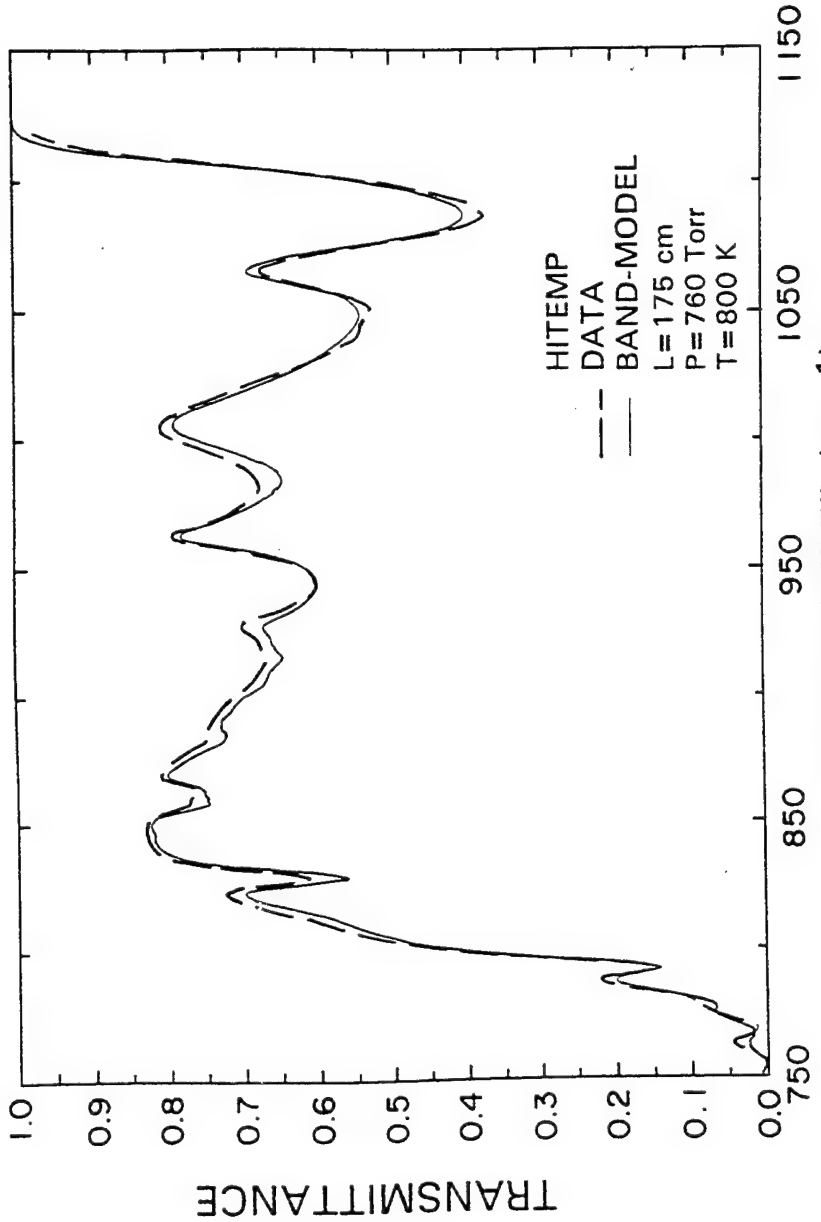

Fig. 2. The 760 torr experimental data are compared to a statistical band-model calculation using the HITEMP data.

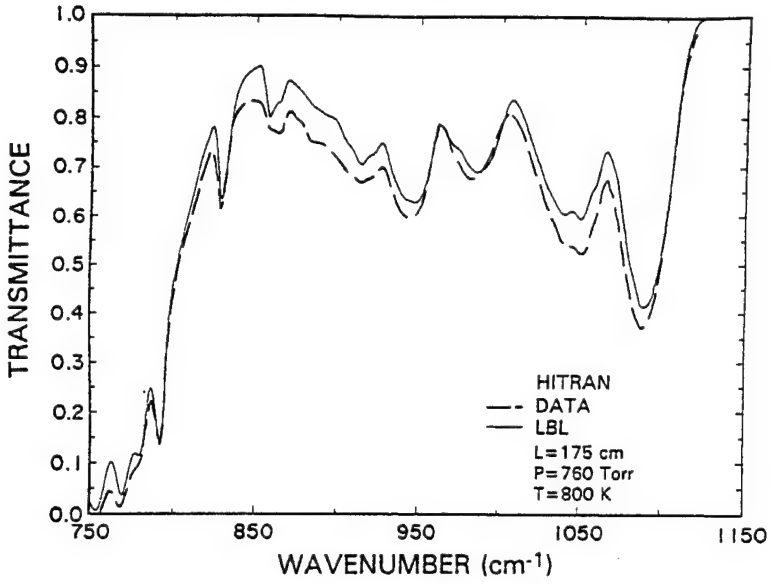

Fig. 3. 760 torr 5.0 cm^{-1} resolution experimental data are compared to line-by-line (LBL) model calculations using the HITRAN data set.

line-by-line code for the HITRAN calculations, while more than 50,000 CO_2 lines were processed using the HITEMP data. As shown in Fig. 3, the line-by-line calculation using the HITRAN line parameter data exhibits about a 10% predicted decrease in absorption compared with the experimental data, just as was found for the band-model comparisons.

As displayed in Fig. 4, there is good agreement between the experimental data and the line-by-line calculations using the HITEMP data. However, in some regions of the spectrum there remains a small discrepancy, especially for the P and R branches of the laser bands at 960 and 1060 cm^{-1}. Next the assumption of constant line width as a function of J for all lines in the

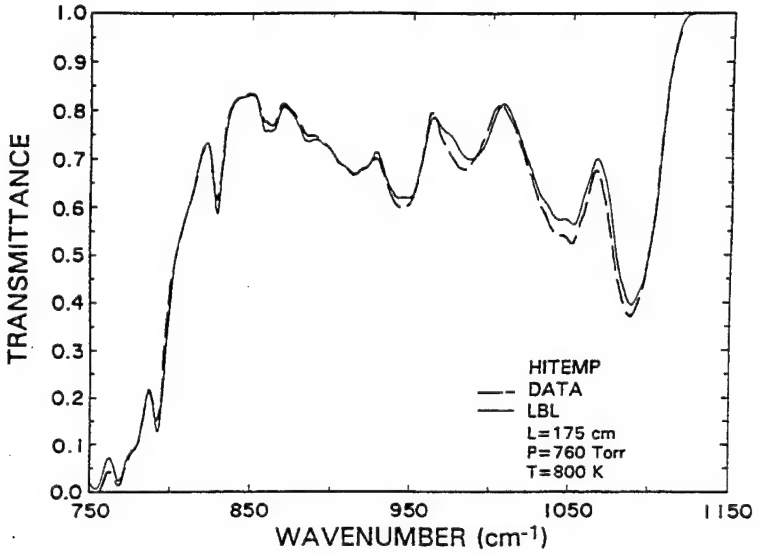

Fig. 4. 760 torr 5.0 cm^{-1} resolution experimental data are compared to line-by-line model calculations using the HITEMP data set.

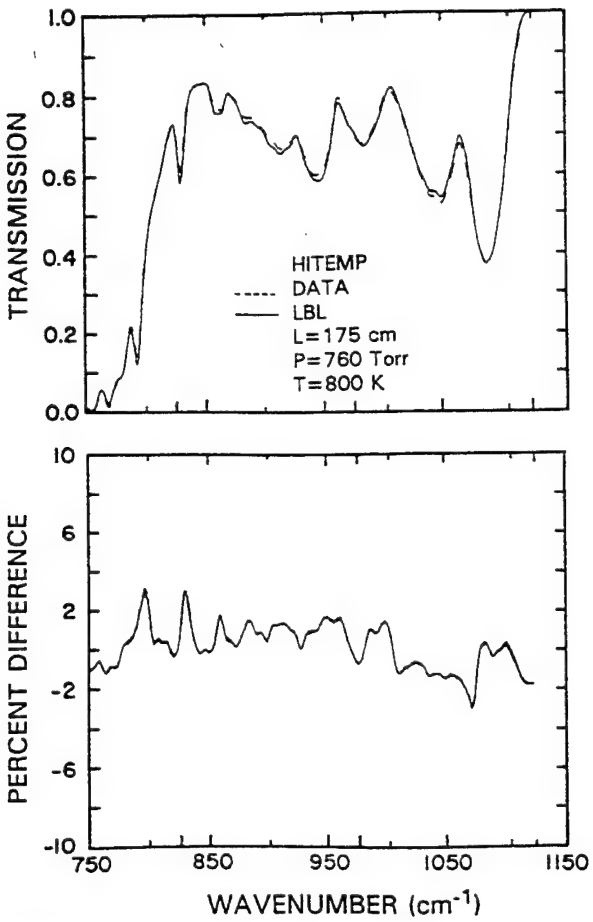

Fig. 5. The J-dependent half-width line-by-line (LBL) transmission calculation and data are compared. The lower panel displays the percent difference between the two curves shown in the upper panel.

line-by-line calculation was removed and the calculation was performed using J-dependent rotational line widths. The variation of the width of the rotational lines as a function of the rotational quantum number for $T = 296\,K$ was obtained from the HITRAN data base. The J-dependent line widths were calculated for $T = 800$ K and resulted in the transmission calculation shown in Fig. 5. The calculation is in excellent agreement with the data and the difference is well within the experimental uncertainty due to temperature variations in the cell and calibration uncertainties. The square-root power-law dependence on the ratio of temperatures for the calculation of the Lorentz width was changed to a 3/4 power law as suggested by Taine,[12] but only marginal improvement resulted from this change.

SUMMARY

This work resulted in the use of the HITEMP data to generate high temperature band-model parameters[6] for use with systems codes under the DNA program. The HITEMP band intensity lists were validated at the temperature of 800 K for the spectral range from 650 to 1200 cm^{-1}.

Acknowledgements—This work was sponsored in large part by the Air Force Systems Command through the Geophysics Directorate of the Phillips laboratory contract F19628-87-C-0208, and the Defense Nuclear Agency through the Atmospheric Effects and Sensor Operability Program contract DNA001-88-C-0030. Also thanks go to Drs John DeVore, John Generosa, and Richard Harris of Physical Research Inc., for many useful discussions.

REFERENCES

1. C. B. Ludwig, W. Malkmus, J. E. Reardon, and J. A. L. Thomson, *Handbook of Infrared Radiation From Combustion Gases*, NASA SP-3080, National Aeronautics and Space Administration, Washington, DC.
2. R. B. Wattson and L. S. Rothman, *J. Molec. Spectrosc.* **199,** 83 (1986).
3. H. Sakai, in *Spectrometric Techniques*, Vol. 1, G. A. Vanasse, ed., Chap. 1, Academic Press, New York, NY (1977).
4. W. S. Dalton and H. Sakai, *Appl. Opt.* **19,** 2413 (1980).
5. L. S. Rothman, *Appl. Opt.* **25,** 1795 (1986).
6. R. A. Parker, Final report, Geophysics Directorate of the Phillips Laboratory, Hanscom AFB, MA 01731.
7. M. P. Esplin and L. S. Rothman, *J. Molec. Spectrosc.* **100,** 193 (1983).
8. M. P. Esplin and L. S. Rothman, *J. Molec. Spectrosc.* **116,** 351 (1986).
9. M. P. Esplin and M. L. Hoke, *JQSRT* **48,** 573 (1992).
10. S. J. Young, *JQSRT* **18,** 1 (1977).
11. A. Coppalle and P. Vervish, *JQSRT* **33,** 465 (1985).
12. J. Taine, *JQSRT* **30,** 371 (1983).

Appendix C

Carbon Dioxide Line Positions in the 780 to 940 Wavenumber Region

Carbon Dioxide Line Positions in the 780 to 940 Wavenumber Region

Mark P. Esplin

Stewart Radiance Laboratory, Utah State University, 139 The Great Road, Bedford, Ma 01730, USA.

Michael Hoke

Geophysics Laboratory (AFSC)/OPS, Hanscom AFB, Bedford, Ma 01730, USA.

ABSTRACT

Spectra of a 40 torr CO_2 sample heated to 800K has been recorded at high resolution in the 780 to 940 cm^{-1} spectral region using the Air Force Geophysics Laboratory high resolution interferometer. A total of 8 different rotation-vibration bands were identified. The measured line positions were used in a least-squares-fit to obtain updated rotation-vibration constants.

1. INTRODUCTION

The high resolution interferometer was used in conjunction with a high temperature absorption cell to carry out a continuing measurement program of high temperature CO_2 in several different wavelength regions[1,2,3]. The spectral region covered by the present paper (780 to 940 cm^{-1}) is just beyond the high wavenumber edge of the ν_2 CO_2 fundamental. The absorptivity of CO_2 is very low in this spectral region at room temperature, but raising the temperature to 800K populates many additional rotation-vibration states, greatly increasing the absorptivity.

2. EXPERIMENTAL DETAILS

The high resolution interferometer is a Michelson interferometer that employs cat's eye retroreflectors and a step and integrate mirror motion. For these measurement, the maximum optical path length used was 1 meter, resulting in an unapodized resolution of 0.005 cm^{-1}. Several spectra were taken under identical experimental conditions, checked for consistency, and then coadded to increase signal to noise. In addition to the CO_2 spectra, the spectrum of the empty cell was also measured. The coadded CO_2 spectrum was then ratioed with the empty cell spectrum to remove the channel spectrum and take out the background.

The 40 torr CO_2 sample was contained in a single pass stainless steel high temperature absorption cell. The total absorption path was 1.75 meters. The central 1 meter section of the cell was maintained at 800K, while the temperature dropped to near room temperature at the ends of the cell where ZnSe windows were located. Since only measurements of spectral line positions, and not line strengths or widths, were the object of this study, no attempt was made to characterize the temperature gradients. The sample cell is connected to the interferometer chamber with a short bellows, approximately 5 cm in length, to allow for expansion of the hot cell. This 5 cm optical path, the only portion of the optical path which is not evacuated, is purged with dry nitrogen.

 0-8194-0706-2/92/$4.00

3. RESULTS

The rotation-vibration bands that were identified in the experimental spectra are indicated by arrows on the CO_2 energy level diagram of figure 1. A least-squares fit to the measured line positions resulted in the molecular constants given in table I. Each band was fit independently with no attempt to make a global CO_2 energy level fit. Figures 2 and 3 show residual plots for the 14401 ← 05501 band. Fig. 2 is for the P and R-branches and Fig. 3 is for the Q-branch. The rotation-vibration constants used in the 1986 HITRAN database[4] and those obtained by Richard Wattson[5] from a DND (direct numerical diagonalization) calculation are also indicated on these figures. The present results were not compared to the 1991 HITRAN database[6] as the present molecular constants have already been incorporated into that database.

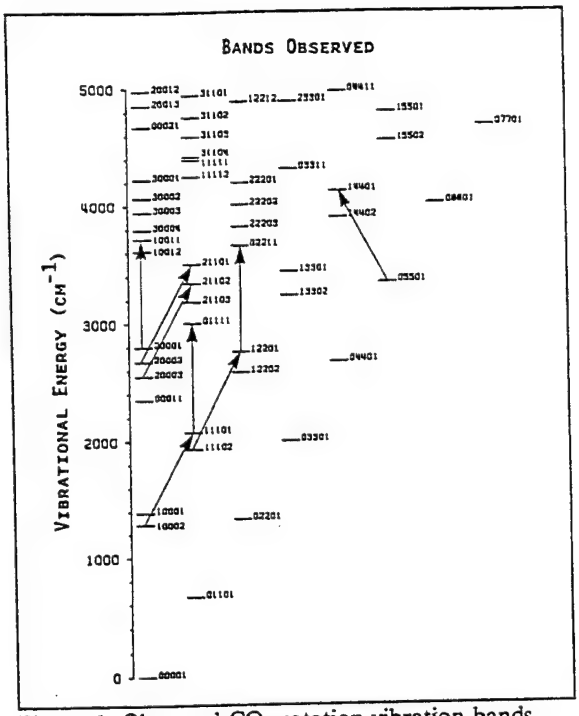

Figure 1. Observed CO_2 rotation-vibration bands

4. ACKNOWLEDGEMENT

This work was supported by the Air Force Office of Scientific Research (AFOSR) as part of GL task 2310G1.

Table I. Rotation-Vibration Constants (cm^{-1})

Transition		Band Center	B'	D'x10^7	H'x10^{13}	B"	D"x10^7	H"x10^{13}
14401	05501	781.7399	.39286673	1.39985		.39376912	1.45111	
21102e	20003	790.9886	.39003464	1.35614	-1.6974	.39110912	1.79262	1.5491
21102f			.39117332	1.36036	-1.8779			
11101e	10002	791.4472	.39040970	1.25693	.6953	.39048219	1.56870	1.8676
11101f			.39133380	1.20910	.2471			
12201e	11102e	828.2535	.39155578	1.47420	4.1508	.39075242	1.55608	13.1083
12201f	11102f		.39155578	1.34139	11.9541	.39169731	1.61884	12.0884
21101e	20002	829.5290	.39035243	.94662		.38952507	1.09417	
21101f			.39167979	.84649				
02211e	12201e	898.5467	.38863900	1.38552	.7975	.39154984	1.43620	-2.8764
02211f	12201f		.38863900	1.39409	5.4035	.39154984	1.29659	5.3820
10011	20001	917.6459	.38709724	1.65222		.39064079	1.44636	
01111e	11101e	927.1557	.38758787	1.58655		.39040662	1.48330	
01111f	11101f		.38818930	1.31813		.39133204	1.17040	

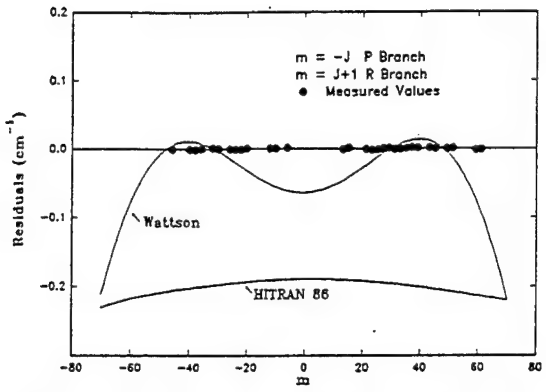

Figure 2. Residual plot for 14401f ← 05501f P and R-Branches

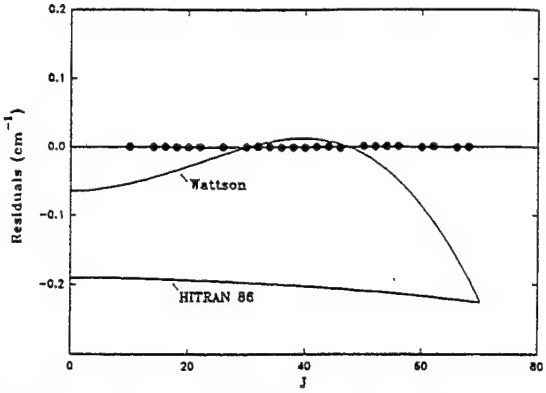

Figure 3. Residual plot for 14401e ← 05501f Q-Branch

5. REFERENCES

1. M.P. Esplin and L.S. Rothman, "Spectral Measurements of High Temperature Isotopic Carbon Dioxide in the 4.3-μm Region," *J. Mol. Spectroscopy* Vol. **100**, 193 (1983).

2. Mark P. Esplin, William M. Barowy, Ronald J. Huppi, and George A. Vanasse, "High Resolution Fourier Spectroscopy of Nitrous Oxide at Elevated Temperatures," *Mikrochim. Acta [Wien]* II, 403 (1988).

3. M.P. Esplin, R.B. Wattson, M.L. Hoke, R.L. Hawkins, and L.S. Rothman, "Observation and Calculation of Carbon Dioxide Bands with High Vibrational Angular Momentum," *Appl. Opt.*, Vol. **28**, 409 (1989).

4. L.S. Rothman, R.R. Gamache, A. Goldman, L.R. Brown, R.A. Toth, H.M. Pickett, R.L. Poynter, J.-M. Flaud, C. Camy-Peyret, A. Barbe, N. Husson, C.P. Rinsland, and M.A.H. Simith, "The HITRAN Database: 1986 Edition," *Appl. Opt.*, Vol. **26**, 4058 (1987).

5. R. B. Wattson and L. S. Rothman, "Determination of Vibrational Energy Levels and Parallel Band Intesities of $^{12}C^{16}O_2$ by Direct Numerical Diagonalization," *J. Mol. Spectrscopy*, Vol. **119**, 83-100.

6. Laurence S. Rothman, "Where we are: Commentary on the Current Edition of HITRAN," Conference of Molecular Spectroscopic Databases, Hanscom Air Force Base, 13-14 June 1991.

Appendix D

Band Centers and Line Positions of Hot Bands of $^{13}C^{16}O_2$ and $^{16}O^{13}C^{18}O$ in the 15 Micron Region

BAND CENTERS AND LINE POSITIONS OF HOT BANDS OF $^{13}C^{16}O_2$ AND $^{16}O^{13}C^{18}O$ IN THE 15 MICRON REGION

Mark P. Esplin
Stewart Radiance Laboratory, Utah State University
139 The Great Road, Bedford MA 01730

Michael Hoke
Geophysics Directorate, Hanscom AFB, 01731

INTRODUCTION

A high-resolution interferometer and high-temperature absorption cell have been used in a continuing measurement program of rotation-vibration spectra of the isotopes of carbon dioxide in different spectral regions. This paper covers results for the isotopes $^{13}C^{16}O_2$ and $^{16}O^{13}C^{18}O$ with band centers in the spectral region 600 to 800 cm^{-1}.

Only a few experimental details will be given here; additional details may be found in the literature.[1] The experimental components include an infrared source, a radiation chopper, a high-temperature single-pass gas-sample absorption cell, a Michelson interferometer with "cat's eye" mirrors employing a step-and-integrate mirror motion, and two liquid-helium-cooled detectors. A carbon dioxide gas sample was contained in the 1.75 meter single-pass stainless-steel sample cell. The central one meter section of the cell was maintained at a temperature of 800K, with temperature gradients in the end segments of the cell, ending with the cell windows at room temperature. For this study a stepping mirror displacement of 75 cm was used, giving a resolution (FWHM) of 0.006 cm^{-1} with triangular apodization.

Three high-resolution interferograms were collected under identical experimental conditions. A single 5 Torr sample of isotopically enhanced carbon dioxide, containing approximately 88 percent $^{13}C^{16}O_2$, 11 percent $^{16}O^{13}C^{18}O$, and 1 percent $^{12}C^{16}O_2$, was maintained in the sample cell at a temperature of 800K throughout the data collection. After apodization the three interferograms were Fourier transformed, checked for consistency and then co-added to yield a single composite spectrum. This spectrum was then ratioed with a low-resolution empty-cell spectrum to produce a transmittance spectrum which was then used for the determination of spectral line positions.

RESULTS

Spectra of high temperature gas samples are much more dense with spectral lines than data collected at room temperature. Consequently, techniques have been developed for the analyses of dense spectral data.[2] In the preliminary analysis discussed here, more than 4000 spectral line positions associated with 24 rotation-vibration bands of the $^{13}C^{16}O_2$ isotope, and 900 spectral lines associated with 4 bands of the $^{16}O^{13}C^{18}O$ isotope have been measured. The vibrational transitions associated with the $^{13}C^{16}O_2$ isotope are shown in Fig. 1. The band identifications and measured band centers are given in Table 1, columns 1 and 2. Five of the $^{13}C^{16}O_2$ transitions, those marked with a (†), have been measured previously by other researchers, and data for these bands have now been incorporated in the HITRAN data base.[3] Also included in Table 1 are comparisons of the observed band centers with those from other sources, including the HITRAN[4] data base (column 3), those determined by Wattson and Rothman[5] (column 4), and those calculated by Chedin and Teffo[6] (column 5). The comparisons are in the form of differences from the observed band center estimates reported in column 2 of Table 1. In some cases the Observed and HITRAN band centers agree quite well (column 3), including transitions between higher vibrational states such as 21101 ← 20001 (0.0014 cm^{-1}), while in other cases the agreement is much worse, for example 21103 ← 20003 (-0.0372 cm^{-1}). This results because some of the energy levels shown in Fig. 1 have been previously determined,[4] by us or other researchers, from transitions in other spectral regions, and that information has already been incorporated within the HITRAN data base. The agreement between the Observed band centers and those of Wattson (column 4) is much more uniform and in many cases is comparable to or better than the agreement between the Observed and HITRAN band centers.

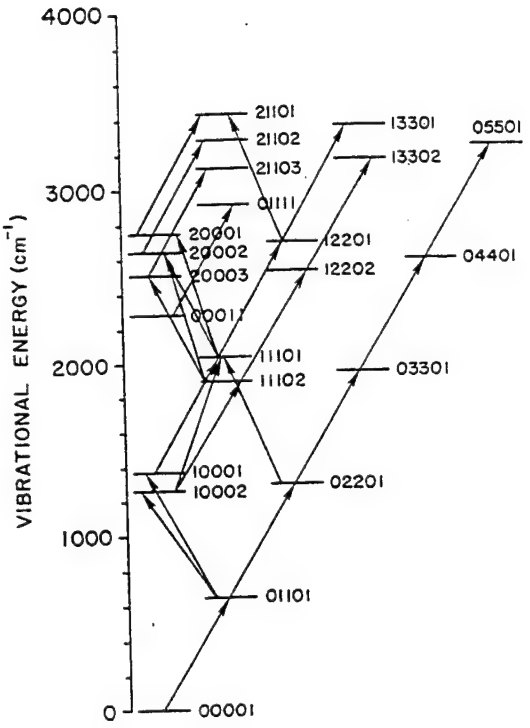

Figure 1. Observed $^{13}C^{16}O_2$ transitions.

Table 1. Observed band centers compared to values determined by other researchers

$^{13}C^{16}O_2$			Comparison With Other Researchers		
Band		Observed	HITRAN91	Wattson	Chedin
20002	11101	607.9669	-.0076	-.0021	.0179
20003	11102	610.9861	-.0055	-.0104	-.0349
10002	01101	617.3494†	-.0004	-.0195	.0014
21103	20003	619.7866	-.0372	-.0096	-.0594
11102	10002	630.7100	-.0002	-.0172	-.0300
12202	11102	635.1375	-.0026	-.0168	-.0575
01111	00011	636.7515	.0007	.0085	-.0065
13302	12202	637.7206	-.0429	-.0061	-.0974
21102	20002	644.6391	.0058	-.0161	-.0039
01101	00001	648.4775†	-.0005	.0130	-.0075
02201	01101	648.7861†	.0009	-.0047	-.0039
03301	02201	649.0865†	-.0002	-.0186	-.0195
04401	03301	649.3778	-.0312	-.0259	-.0552
05501	04401	649.6614	-.0260	-.0209	-.1086
13301	12201	661.1392	.0039	-.0034	-.0778
12201	11101	663.1709	-.0002	-.0089	-.0361
11101	10001	667.0313	.0001	-.0019	-.0177
21101	20001	683.1757	.0014	-.0193	.0297
20001	11101	713.5029	-.0002	.0012	.0549
10001	01101	721.5836†	-.0005	-.0218	-.0044
21101	12201	733.5077	.0014	-.0092	.1207
11101	02201	739.8285	-.0016	-.0193	-.0185
20002	11102	748.5232	-.0067	.0117	.0252
11101	10002	771.2654	-.0002	-.0043	-.0236
$^{13}C^{16}O^{18}O$			Comparison With Other Researchers		
Band		Observed	HITRAN91	Wattson	Chedin
10002	01101	601.5814	.0102		-.0026
01101	00001	643.3186	-.0104		-.0094
02201	01101	643.6544	.0014		-.0046
10001	01101	698.9586	.0098		-.0064

†Bands known to have been observed previously[4].

The band center and line position estimates of Wattson are based on a technique for Direct Numerical Diagonalization (DND) of an appropriate Hamiltonian.[7] In this technique a molecular coordinate system, an approximate potential energy surface, and a set of basis functions are chosen and from these a numerical Hamiltonian is computed and then iteratively diagonalized and fit to a set of experimentally determined rotation-vibration energy levels using a non-linear least-squares fitting routine to adjust the potential energy parameters. From the derived potential function, previously unknown energy levels, and from these rotational-vibrational line positions, may be predicted. The technique has been applied to the $^{12}C^{16}O_2$ isotope using as input some of the results determined earlier as part of our measurement program. The band centers and line positions estimated by Wattson[5] and used in our current study were not determined using experimental data for the $^{13}C^{16}O_2$ isotope, because very little data existed for this isotope. Instead the results for this isotope were obtained by employing an isotopic shift and using only data for the principal isotope $^{12}C^{16}O_2$.

Figure 2 shows comparisons of rotational line positions for the 20002 ← 11102e transition of $^{13}C^{16}O_2$. The data are presented as line position differences. The solid black dots are the observed positions minus the positions determined from a linear-least-squares fit of the measured positions. The expression used in the fit to represent the line positions was $\upsilon(J) = E'_{v'}(J) - E''_{v''}(J)$ where $E'_{v'}(J)$ and $E''_{v''}(J)$ are given in terms of the rotational constants B_v ,D_v ,and H_v by the following expression:

$$E_v(J) = G_v + B_v [J(J+1)] - D_v [J(J+1)]^2 + H_v [J(J+1)]^3.$$

Line position differences calculated using our rotational constants are compared, in Fig. 2, to the line positions in the HITRAN[4] data base, those determined by Wattson,[5] and those calculated by Chedin[6]. As the figure shows, the new measurements are an improvement over the HITRAN values, for this band, for rotational quantum numbers above 40. The same pattern was found for most of the other measured bands; above some J value the differences grow large very fast. However, for some of the measured transitions, significant differences were found for all values of J. Because the results of Wattson (marked "Wattson" in Fig. 2) were determined using only data for the principal isotope $^{12}C^{16}O_2$ and not the isotope under study, $^{13}C^{16}O_2$, the comparison in Fig. 2 is very impressive. The result seen in Fig. 2 in which the agreement, between the line positions of Wattson and the measured line positions, is better at high J values than the agreement between the measured line positions and the HITRAN line positions, is a general characteristic found for many of the measured transitions. It reflects constraints on the calculations by Wattson for the express purpose of enhancing the high J results for which the data in the HITRAN data base may not be adequate, as the curve in Fig. 2 marked "HITRAN" illustrates. Figure 2 also shows the general pattern for the comparisons with the positions calculated by Chedin[6]; the agreement is better for low J values than for high J values; but as the figure suggests, the agreement is generally not very good.

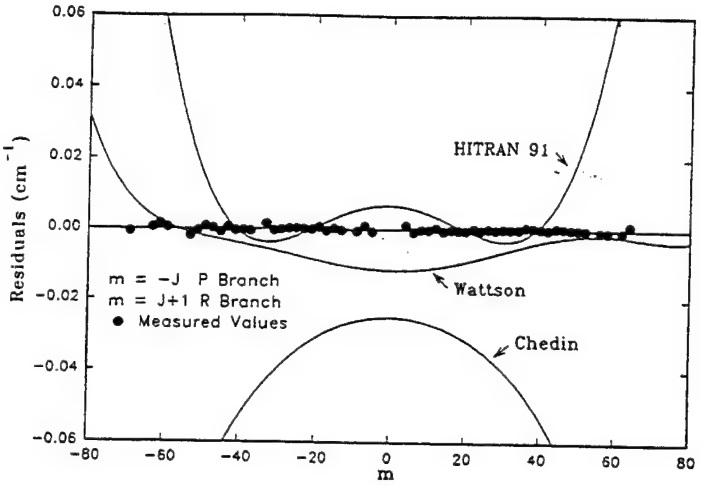

Figure 2. Line position differences for the P and R branches of the 20002 ← 11102e band of $^{13}C^{16}O_2$.

The presentation here is preliminary. Analysis of spectral data taken at a pressure of 20 Torr must still be combined with the results from the analysis of the 5 Torr data. Complete results and estimates of band centers, line positions and from these rotational constants will be presented.

REFERENCES

1. M.P. Esplin, R.J. Huppi, and G.A. Vanasse, "Spectral Measurements of High Temperature $^{13}C^{16}C_2$ and $^{13}C^{16}O^{18}O$ in the 4.3 μm region", Appl. Opts. 21, 1681(1982).

2. M.P. Esplin and M.L. Hoke, "Hot Bands of Carbon Dioxide in the 15 Micron Region" in High Resolution Fourier Transform Spectroscopy, Optical Society of America 1989 Technical Digest Series Vol. 6, pp27(1989).

3. L.S. Rothman, R.L. Hawkins, R.B. Wattson, and R.R. Gamache, "Energy Levels and Intensities of Atmospheric Carbon Dioxide Bands", JQSRT (in press 1992).

4. L.S. Rothman, "HITRAN Molecular Database: Editions of 1991 and 1992", JQSRT (in press 1992).

5. R.B. Wattson, Private Communication, 1992.

6. A. Chedin and Jean-Luc Teffo, "The Carbon Dioxide Molecule: A New Derivation of the Potential, Spectroscopic, and Molecular Constants," J. Mol. Spec. 107, 333(1984).

7. R.B. Wattson and L. S. Rothman, "Determination of Vibrational Energy Levels and Parallel Band Intensities of $^{12}C^{16}O_2$ by Direct Numerical Diagonalization", J. Molec. Spec. 119, 83(1986).

Appendix E

Line Positions From High Temperatures Isotopically Enriched CO_2 in the 740 to 1060 cm^{-1} Region

LINE POSITIONS FROM HIGH TEMPERATURE ISOTOPICALLY ENRICHED CO_2 IN THE 740 TO 1060 cm^{-1} REGION

Mark P. Esplin
Stewart Radiance Laboratory, Utah State University, 139 The Great Road, Bedford, Ma. 01730

ABSTRACT

A high resolution step-and-hold Fourier transform spectrometer has been used to observe the spectrum of CO_2 samples heated to 800K in a high temperature absorption cell. The interferograms were recorded using a maximum optical path difference of 152 cm resulting in an apodized spectral resolution of 0.007 cm^{-1}. The 20 torr isotopically enriched CO_2 sample consisted of 88 % $^{13}C^{16}O_2$ and 11 % $^{16}O^{13}C^{18}O$. The sample was contained in a single pass high temperature absorption cell with a total absorption path length of 1.75 meters. A total of 1601 lines belonging to 15 rotation-vibration bands of $^{13}C^{16}O_2$ and 146 lines belonging to two bands of $^{16}O^{13}C^{18}O$ were identified in the observed spectrum. A weighted least-squares fit was then used to obtain improved estimates of the band centers and rotational constants.

EXPERIMENTAL SETUP

The experimental components include an infrared source, high temperature gas sample absorption cell and high resolution interferometer. The step-and-hold Michelson interferometer employs "cat's-eye" mirrors and a stepping displacement, for this study, of 76 cm. This corresponds to an unapodized resolution of approximately 0.007 cm^{-1}. The input and output beams of the cat's-eye mirrors are laterally displaced making both accessible. Since the two beams are complementary, two detectors are used and the signals differenced to yield the interferometric signal and reduce the effect of systematic errors, such as source fluctuations and instrumental drifts. The liquid helium cooled detectors are housed in the same dewar to keep their experimental conditions the same. In practice this arrangement is very stable over the twelve to fifteen hour data collection period necessary to collect a single high resolution interferogram. For operation in the fifteen micron spectral region a potassium bromide beam splitter and copper doped germanium detectors were used. The interferometer chamber, which also contains the transfer optics and optical filter wheel, is evacuated during operation. The single pass stainless steel gas sample cell is coupled to the interferometer chamber with a purge expansion bellows. The cell is housed in a commercial electric furnace and for our studies was heated to 800K. The single pass length is 1.75 meters. However only the central one meter portion of the cell was near the furnace temperature, with temperature gradients in the end portions and the zinc selenide cell windows at room temperature. The source chamber contains a Nernst glower, radiation chopper and collimation optics. It is mounted rigidly to the absorption cell and evacuated during operation. The hot gas sample not only absorbs but radiates. Locating the chopper in the source chamber in the optical path before the sample cell prevents the gas emissions from being modulated and recorded. The infrared signals are detected, demodulated and integrated digitally. The digital system provides fast settle down after a moving mirror "step" and long data integration times during the moving mirror "hold".

MEASUREMENTS

Several interferograms of high temperature (800K), low pressure (5 and 20 torr) isotopically enhanced carbon dioxide samples were collected for analyses of the vibrational, rotational bands in the 9 to 17 micron spectral region. Each high resolution interferogram of the 5 torr sample included approximately 400,000 data points, sampling the interferogram every sixth NeHe laser fringe. Figure 1 is a portion of a transmittance spectrum. It is the ratio of a high resolution spectrum and a low resolution empty-cell background spectrum. The loss of instrumental sensitivity is evidenced near 600 cm^{-1}. For comparison, the lower portion of the same figure is a spectrum, collected under similar conditions, using a naturally occuring sample of carbon dioxide. The figure illustrates the differences in the spectral structure of the $^{12}C^{16}O_2$ and $^{13}C^{16}O_2$ isotopes. The upper portion of Figure 2 is a detail of the $^{13}C^{16}O_2$ spectrum shown in Figure 1, showing a smaller spectral region the 5 torr and a comparable portion of a 20 torr spectrum. The slightly higher absorber amount in the 20 torr spectrum allows more spectral lines to be observed with out significant increase in line position measurement error.

RESULTS

Table 1 lists the vibrational transitions and the measured band center of the bands which were investigate in this study. Also listed in the table is the quantum number range of the measured lines in the P and R branches of each band studied, as well as the number of measured lines for each band. A total of 1601 $^{12}C^{16}O_2$ spectral lines were measured and a total of 146 $^{16}O^{13}C^{18}O$ spectral lines were measured. Rotational constants are not given in the table but are available from the authors. To check the analysis, line positions calculated from the estimated rotational constants were compared with the values on HITRAN92[1], the most recent version of the HITRAN line parameter data base. As an example, Figure 3 is a comparision for the well known "laser" band with band center near 913 cm^{-1}. In this figure, the dots represent the differences between the measured line positions and the line positions calculated from the estimated rotational constants. The solid line, marked HITRAN92, represents the differences between the line positions calculated using our estimated rotational constants and the line positions on the HITRAN92 data base. The new measurements provide some improvement for this well-known band, but greater improvement for many of the other bands listed in the table.

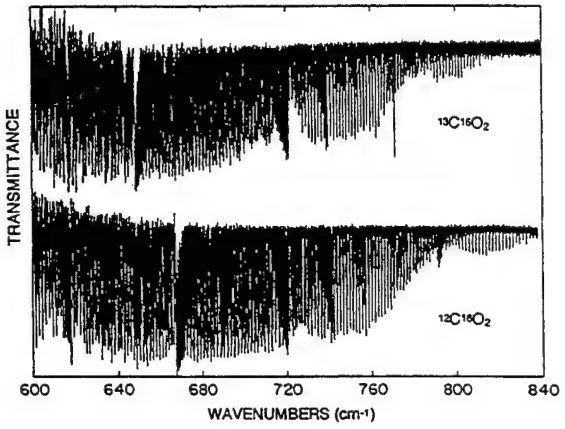

Figure 1 Transmittance spectra of 800K, 5 Torr carbon dioxide.

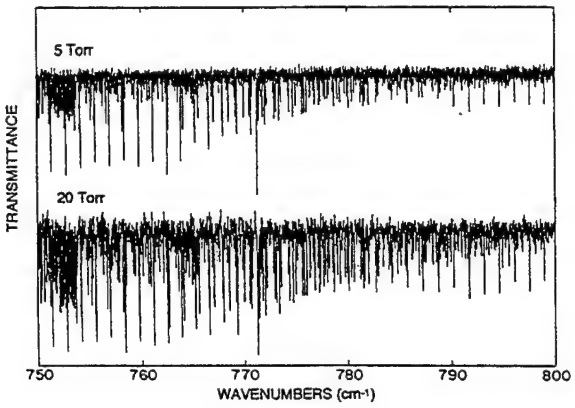

Figure 2 Transmittance spectra of 5 Torr and 20 Torr samples of $^{13}C^{16}O_2$

Table I Rovibrational transition investigated in this study.

$^{13}C^{16}O_2$			Results of Least-squares-fits				
Band		Band Center	Range of Measurement			Number of lines	RMS error x10^4
11101e	02201e	739.6287	P(76)	Q(52)	R(92)	227	2
11101f	02201f		P(69)	Q(65)	R(87)		
20002	11102e	748.5231	P(69)		R(67)	105	3
	11102f			Q(76)			
12201e	03301e	753.9127	P(45)	Q(61)	R(79)	183	3
12201f	03301f		P(44)	Q(76)	R(82)		
21102e	12202e	758.0246	P(24)	Q(44)	R(58)	101	7
21102f	12202f		P(43)	Q(35)	R(61)		
13301	04401	765.6736	P(54)	Q(67)	R(80)	128	6
11101	10002	771.2654	P(66)	Q(54)	R(82)	103	3
21102	20003	782.1762	P(44)	Q(56)	R(54)	60	8
21101	20002	786.7121	P(36)	Q(46)	R(40)	32	5
12201e	11102e	803.7266	P(23)	Q(43)	R(41)	72	7
12201f	11102f		P(40)	Q(46)	R(46)		
02211e	12201e	857.0501	P(46)		R(58)	82	8
02211f	12201f		P(45)		R(57)		
10011	20001	862.3133	P(68)		R(76)	60	6
01111e	11101e	883.1444	P(67)	Q(0)	R(71)	137	4
01111f	11101f		P(70)	Q(0)	R(76)		
00011	10001	913.4250	P(66)		R(94)	85	2
00011	10002	1017.6592	P(68)		R(62)	84	2
01111e	11102e	1023.7005	P(77)	Q(0)	R(77)	142	3
01111f	11102f		P(80)	Q(0)	R(74)		

$^{16}O^{13}C^{18}O$			Results of Least-squares-fits				
Band		Band Center	Range of Measurement			Number of lines	RMS error x10^4
00011	10001	923.6939	P(51)		R(53)	67	9
00011	10002	1021.0714	P(52)		R(49)	79	8

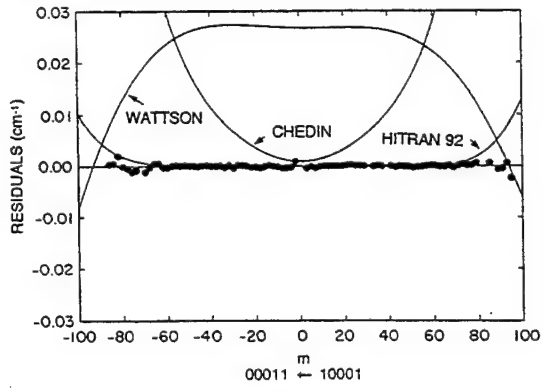

Figure 3 Comparison of measured line positions and line positions from HITRAN92 and positions calculated from rotational constants.

ACKNOWLEDGEMENTS

This work was supported by the Air Force Office of Scientific Research (AFOSR) as part of GL task 2310G1.

REFERENCES

1. L.S. Rothman et al, "The HITRAN molecular database: editions of 1991 and 1992", JQSRT, 48, 469(1992).

Appendix F

The Rovibrational Intensities of the $(40^{0}1) \leftarrow (00^{0}0)$ Pentad of $^{12}C^{16}O_2$ between 7284 and 7921 cm^{-1}

JOURNAL OF MOLECULAR SPECTROSCOPY 175, 104–111 (1996)
ARTICLE NO. 0014

The Rovibrational Intensities of the $(40^01) \leftarrow (00^00)$ Pentad Absorption Bands of $^{12}C^{16}O_2$ between 7284 and 7921 cm^{-1}

L. P. Giver,* C. Chackerian, Jr.,* M. N. Spencer,* L. R. Brown,† and R. B. Wattson‡

*NASA Ames Research Center, Moffett Field, California 94035-1000; †Jet Propulsion Laboratory, California Institute of Technology, Pasadena, California 91109; and ‡Stewart Radiance Laboratory, Utah State University, Bedford, Massachusetts 01730

Received July 24, 1995; in revised form October 10, 1995

Absolute line intensities and Herman–Wallis type intensity parameters of $^{12}C^{16}O_2$ are experimentally measured for the first time for the $(40^01)_{IV} \leftarrow (00^00)$ band at 7460 cm^{-1} and the $(40^01)_I \leftarrow (00^00)$ band at 7921 cm^{-1}. The rotationless band strengths at 296 K are respectively

$$S^0_{vib}[IV] = 0.0429(6) \times 10^{-22}\ cm^{-1}/(molecule/cm^2)$$

and

$$S^0_{vib}[I] = 0.00189(6) \times 10^{-22}\ cm^{-1}/(molecule/cm^2).$$

In addition, previous measurements on the $(40^01)_{II} \leftarrow (00^00)$ and $(40^01)_{III} \leftarrow (00^00)$ bands have been reanalyzed to be consistent with definitions of Herman–Wallis parameters currently in use.

INTRODUCTION

Recent observations (1–3) of the nightside near-infrared spectrum of Venus have discovered emission windows between 4040 and 4550 cm^{-1} and between 5700 and 5900 cm^{-1}, as well as several smaller ones between 7500 and 9400 cm^{-1}. Carbon dioxide absorption bands are a major source of near-infrared atmospheric opacity on Venus; these emission windows occur between CO_2 bands where the opacity is low enough to allow radiation from the hot surface to pass through most of Venus' atmosphere. Pollack *et al.* (4) analyzed these emission windows in an effort to improve the determination of the composition and cloud structure of the lower atmosphere of Venus. To facilitate part of this effort, Giver and Chackerian (5) made laboratory measurements of the intensity and Herman–Wallis parameters of the very weak $(31^10)_{IV} \leftarrow (00^00)$ band at 4416 cm^{-1}, which is prominent in Venus' emission window between 4040 and 4550 cm^{-1}. However, modeling the emission spectrum (4) did not produce a good fit for the window centered at 7830 cm^{-1}. The CO_2 bands that are prominent in this region belong to the vibrational sequence $4\nu_1 + \nu_3$ and associated hot bands. In addition, the very weak and perturbed $(21^12)_{II} \leftarrow (00^00)$ perpendicular band contributes some absorption around 7900 cm^{-1}.

For the purpose of orientation and later comparisons, the band centers, rotationless band strengths, and Herman–Wallis intensity factors for the series $n\nu_1 + \nu_3$ are taken from the 1992 HITRAN database (6) and shown in Table 1 for $n = 0$ through $n = 4$. As is apparent from Table 1, the intensity sum of each $n\nu_1 + \nu_3$ polyad is about a factor of 50 weaker than the next lower sequence. Only two of the five bands of the $(40^01) \leftarrow (00^00)$ pentad are based on laboratory intensity measurements (7, 8). Intensity parameters for $(40^01)_I \leftarrow (00^00)$ at 7921 cm^{-1}, $(40^01)_{IV} \leftarrow (00^00)$ at 7460 cm^{-1}, and $(40^01)_V \leftarrow (00^00)$ at 7284 cm^{-1} have not been previously measured. For the 1992 HITRAN database, their rotationless band strengths and Herman–Wallis parameters were predicted from direct numerical diagonalization (DND) calculations (9) which are dependent upon the S^0_{vib} values of measured ground state bands.

For the purpose of this paper, we measured line intensities to obtain dipole moments, rotationless band strengths, and Herman–Wallis terms for the two pentad bands at 7460 and 7921 cm^{-1}. These experimental values can be used to refine the DND calculations for related, unmeasurable bands needed to improve the analysis of Venus' nightside spectrum. Unfortunately, the band at 7284 cm^{-1} is too overlapped by residual H_2O transitions to be measured in these spectra. We have also measured the intensities of some lines of the $(21^12)_{II} \leftarrow (00^00)$ perpendicular band at 7901 cm^{-1} which exhibits a strong rotational perturbation. As yet, we have not modeled these intensity measurements.

Some intensity measurements were made of lines in the previously measured bands at 7734 and 7594 cm^{-1}, to check the tabulated intensities of Valero and Boese (7) and Valero

0022-2852/96 $18.00

TABLE 1
Positions and Intensities of the $n\nu_1 + \nu_3$ Bands of $^{12}C^{16}O_2$

Band	Origin (cm^{-1})	Intensity[a] S^0_{vib}	Herman-Wallis Values[b] A_1	A_2
$(00^01)_I \leftarrow (00^00)$	2349.143	916076.0	-0.00014	0.0
$(10^01)_{II} \leftarrow (00^00)$	3612.841	9861.0	0.00010	1.57 x10^{-5}
$(10^01)_I \leftarrow (00^00)$	3714.782	15223.0	0.00004	-1.14 x10^{-5}
$(20^01)_{III} \leftarrow (00^00)$	4853.623	78.1	0.0008	2.6 x10^{-5}
$(20^01)_{II} \leftarrow (00^00)$	4977.835	347.5	-0.00009	-0.47 x10^{-5}
$(20^01)_I \leftarrow (00^00)$	5099.660	109.0	0.0	0.0
$(30^01)_{IV} \leftarrow (00^00)$	6075.980	0.514	0.0016	2.5 x10^{-5}
$(30^01)_{III} \leftarrow (00^00)$	6227.917	4.52	0.0009	4.2 x10^{-5}
$(30^01)_{II} \leftarrow (00^00)$	6347.852	4.54	0.00095	3.8 x10^{-5}
$(30^01)_I \leftarrow (00^00)$	6503.081	0.586	0.00115	3.8 x10^{-5}
$(40^01)_V \leftarrow (00^00)$	7283.978	0.00401	-0.00019	3.71 x10^{-5}
$(40^01)_{IV} \leftarrow (00^00)$	7460.527	0.0469	-0.00014	2.82 x10^{-5}
$(40^01)_{III} \leftarrow (00^00)$	7593.695	0.102	0.0	0.0
$(40^01)_{II} \leftarrow (00^00)$	7734.448	0.0281	0.00025	0.0
$(40^01)_I \leftarrow (00^00)$	7920.838	0.00175	0.00075	-2.43 x10^{-5}

[a]Intensities in units of 10^{-22} $cm^{-1}/(molecule/cm^2)$ at 296K: from Ref. (6).
[b]Herman-Wallis parameters defined by Eq. 4.

(8). Since our measurements were within 3% of their values, we did not make extensive new measurements of these bands. However, we did refit their measurements in the same manner used in this paper which confirmed the 1992 HITRAN rotationless band strength for the $(40^01)_{III} \leftarrow (00^00)$ transition and the revised value of Valero and Boese (10) for the $(40^01)_{II} \leftarrow (00^00)$ band. In this process we obtained Herman–Wallis parameters consistent with the definitions used for the 1992 HITRAN database.

EXPERIMENTAL DETAILS

We obtained spectra using the Fourier transform spectrometers (FTSs) at NASA Ames and the Kitt Peak National Observatory. Most of our spectra were obtained with the Ames 25-m base-path White-type (11) multiple-traversal absorption cell. Operating in air, radiation from a quartz-halogen lamp was sent through a BOMEM DA3.002 Fourier-transform spectrometer equipped with a quartz beamsplitter. The recombined beam then entered the White cell and subsequently focused onto an InSb detector operating at 77 K and equipped with a cold filter to maximize its sensitivity at >3000 cm^{-1}. The cell was filled with Coleman grade CO_2 with minimum purity of 99.99%. The CO_2 pressures in the White cell were measured with MKS Baratron 10-, 100-, and 1000-Torr manometers with digital readout. A total of 22 spectra from about 7200 to 8000 cm^{-1} were obtained.

In addition to the spectra obtained at Ames, a few spectra of CO_2 in the 3800 to 8400 cm^{-1} region were obtained at Kitt Peak with the McMath FTS. These spectra utilized a 6-m base-path White cell (11); the absorber abundance was large enough on one of these spectra to measure the intensities of some lines of the 7460 cm^{-1} band. In addition, a second short cell placed in series with the White cell was used for CO frequency standards. The experimental conditions of all 23 spectra are given in Table 2.

Since the absorption lines in the 7900 cm^{-1} region are very weak despite the long path lengths, we selected an aperture that limited the resolution to 0.045 cm^{-1} for most of our Ames spectra, which brought the signal/noise to acceptable levels. Interferograms were coadded for three hours and transformed using Hamming apodization. For the higher-pressure spectra listed in Table 2, this instrumental resolution was sufficient to almost fully resolve the true spectra. Several of the lower-pressure Ames spectra were obtained with 0.024 cm^{-1} resolution. Some of these were divided by an empty-cell comparison spectrum to yield transmission spectra. This eliminated some of the room air water vapor features from these spectra. The Kitt Peak spectrum was obtained with an hour integration time using 0.011 cm^{-1}

TABLE 2
Experimental Conditions

Spectrum Number	Path Length (m)	Pressure (torr)	Temperature (K)	Resolution (cm^{-1})
[a]1	193	59.7	298.0	0.011
2	407	60.3	294.8	0.024
3	407	98.1	294.9	0.024
4	407	138.7	295.0	0.024
5	407	138.7	295.0	0.045
6	1207	138.7	294.3	0.024
7	1207	138.7	294.7	0.024
8	1207	338.9	295.1	0.045
9	1507	269.6	294.7	0.045
10	1507	339.1	294.7	0.045
11	1507	339.1	295.1	0.045
12	1607	9.98	294.8	0.045
13	1607	24.58	295.2	0.045
14	1607	49.18	295.0	0.045
15	1607	84.8	294.8	0.045
16	1607	119.7	295.2	0.025
17	1607	128.0	295.1	0.045
18	1607	170.0	294.7	0.045
19	1607	199.9	294.7	0.045
20	1607	230.7	295.2	0.045
21	1607	279.8	295.7	0.045
22	1707	279.9	294.9	0.045
23	1707	360.2	295.0	0.045

[a]Spectrum #1 recorded at the Kitt Peak solar FTS.

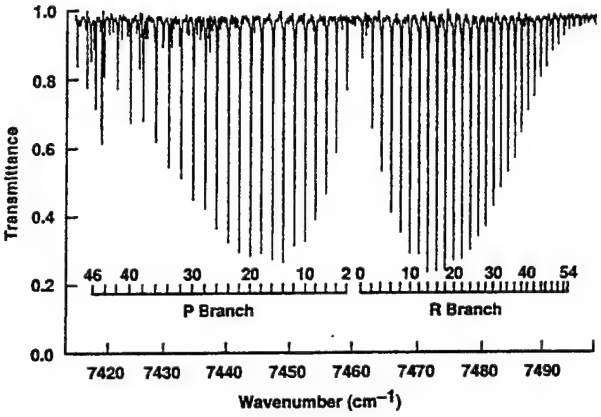

FIG. 1. Transmittance spectrum of the $(40^01)_{IV} \leftarrow (00^00)$ band at 7460 cm^{-1} obtained at Ames, using a total absorption path of 1607 m, a CO_2 pressure of 170.0 Torr, and a temperature of 294.7 K. Individual *P*- and *R*-branch transitions are identified. The spectral features that are not part of this band are primarily incompletely canceled water lines in the room air path between the absorption cell and the Bomem FTS.

resolution and transformed with the weak "Brault" apodization (see Spencer *et al.* (12)). The $(40^01)_{IV} \leftarrow (00^00)$ band at 7460 cm^{-1} is displayed in Fig. 1 and the $(40^01)_I \leftarrow (00^00)$ band at 7921 cm^{-1} is displayed in Fig. 2.

Line intensities were determined using nonlinear least-squares fitting of the spectra (12). Line profiles were computed using the laboratory conditions for each spectrum, the instrumental profile and the self-broadening coefficient for each line as given by Rothman *et al.* (6). These self-broadening coefficients are a parameterized fit to several sets of pressure broadening measurements on stronger CO_2 bands, which were assumed to be independent of vibrational transition. These self-broadening coefficients were revised by up to 10% from the 1986 HITRAN values (13). Since the pentad bands we are measuring are quite weak, we did not attempt to measure their self-broadening parameters. However, before accepting the new coefficients of Rothman *et al.* (6), we did measure the self-broadening coefficients of lines in the $(30^01)_I \leftarrow (00^00)$ band at 6503 cm^{-1} using two spectra obtained with the Kitt Peak FTS. This stronger band was chosen since the lines have between 30 and 80% central absorption, which is optimal for self-broadening determinations; the signal-noise was very high in this region. These measured values agreed with the 1992 HITRAN (6) parameterization to within our experimental uncertainty of ±3%. Thus, these measurements support the revision of the 1986 HITRAN self-broadening coefficients.

Having adopted the self-broadening coefficients from Rothman *et al.* (6), lines of the pentad bands were fitted individually wherever possible. For each small spectral interval, the position and intensity of the line were adjusted for the calculated spectrum until the sum of the squares of the differences between the observed and calculated line profiles was minimized. In cases of overlapping lines in the spectral interval it was necessary to fit two or more lines simultaneously. Residual water vapor lines in the region of the 7460 cm^{-1} band also had to be included in this fitting procedure; only a few CO_2 lines had to be omitted because of serious water vapor contamination. During the fitting procedure for each small spectral interval, the calculated spectrum included lines outside the interval, holding the parameters of these lines fixed at their approximate values.

Line intensities were determined in units of $cm^{-1}/(molecule/cm^2)$ at the temperature of each spectrum, using the total measured pressure and path length without correction for isotopic abundance. These line intensities for each spectrum were then standardized to 296 K so the line measurements from different spectra could be averaged. The averaged line intensities, S_{obs}, are presented in Tables 3 and 4 for each of the pentad bands measured. These values are consistent with the HITRAN definition for intensities in a gas with a standard mixture of its isotopomers. Line intensities appropriate for a gas of the pure $^{12}C^{16}O_2$ isotopomer can be obtained by dividing these tabulated values of S_{obs} by the isotopic fraction, $f = 0.9842$.

DATA ANALYSIS

The rotationless transition moment squared and Herman-Wallis intensity parameters for each band were obtained from the measured line intensities standardized to 296 K via the theoretical expression for the individual line intensities,

$$S_{J''} = \{8\pi^3 10^{-36}/[3hcQ_{vr}(T)]\} \times \{\sigma f \exp(-E''hc/kT)\} L_{J''} |R_{vib}|^2 F(m), \quad [1]$$

where the line intensity is in units of $cm^{-1}/(molecule/cm^2)$,

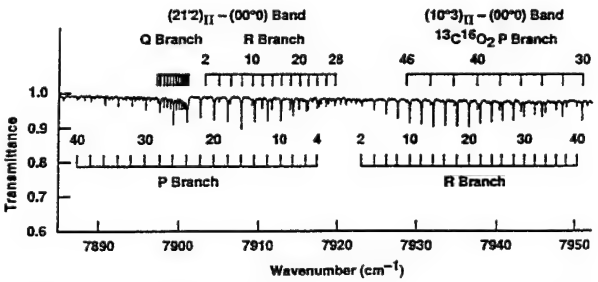

FIG. 2. Transmittance spectrum of the $(40^01)_I \leftarrow (00^00)$ band at 7921 cm^{-1} obtained at Ames, using a total absorption path of 1707 m, a CO_2 pressure of 279.9 Torr, and a temperature of 294.9 K. Individual *P*- and *R*-branch transitions are identified. *Q*- and *R*-branch lines of the $(21^12)_{II}$–(00^00) band at 7901 cm^{-1} are also identified on this spectrum, but the *P*-branch lines of this band are too weak to observe. In addition, *P*30 through *P*46 of the $^{13}C^{16}O_2$ band at 7981 cm^{-1} are marked on this spectrum.

TABLE 3
Rovibrational Line Intensities for the $(40^01)_I \leftarrow (00^00)$ Band of $^{12}C^{16}O_2$

Line	$\sigma(cm^{-1})^a$	n[b]	wt[c]	S_{obs}[d]	$2\Delta S\%$[e]	S_{cal}[d]	$(S_{obs}-S_{cal})/S_{cal}$ (%)
P 38	7889.024	4	1.81	0.0137	8.2	0.0131	5.0
P 36	7890.793	12	3.22	0.0170	6.2	0.0168	1.3
P 34	7892.553	10	2.60	0.0223	6.9	0.0211	5.4
P 32	7894.305	11	10.63	0.0225	3.4	0.0261	-13.6
P 30	7896.048	12	11.35	0.0344	3.3	0.0316	8.7
P 28	7897.781	12	9.12	0.0352	3.7	0.0375	-6.2
P 22	7902.920	12	12.0	0.0547	1.4	0.0549	-0.4
P 20	7904.611	12	12.0	0.0613	2.1	0.0595	3.0
P 18	7906.290	12	12.0	0.0636	2.7	0.0628	1.2
P 14	7909.612	12	12.0	0.0655	2.5	0.0641	2.1
P 12	7911.255	12	12.0	0.0656	1.8	0.0615	6.7
P 10	7912.885	9	9.0	0.0559	2.2	0.0564	-0.9
P 8	7914.502	12	12.0	0.0537	1.6	0.0488	9.9
P 6	7916.106	12	11.78	0.0374	3.2	0.0390	-4.2
P 4	7917.696	10	3.68	0.0258	5.8	0.0273	-5.5
R 4	7924.690	11	6.04	0.0304	4.5	0.0348	-12.6
R 6	7926.208	12	9.59	0.0428	3.6	0.0468	-8.5
R 8	7927.712	11	11.0	0.0568	2.6	0.0570	-0.3
R 10	7929.203	11	11.0	0.0665	1.8	0.0648	2.7
R 12	7930.681	11	11.0	0.0713	1.8	0.0702	1.5
R 14	7932.147	11	11.0	0.0758	1.6	0.0731	3.7
R 16	7933.599	11	11.0	0.0746	1.6	0.0735	1.5
R 18	7935.040	10	10.0	0.0703	2.2	0.0718	-2.1
R 20	7936.468	12	12.0	0.0680	2.4	0.0682	-0.4
R 22	7937.884	12	12.0	0.0606	2.3	0.0632	-4.2
R 24	7939.289	10	10.0	0.0542	2.9	0.0573	-5.4
R 26	7940.682	11	11.0	0.0508	3.3	0.0507	0.2
R 28	7942.065	8	8.0	0.0490	2.1	0.0440	11.4
R 30	7943.439	11	11.0	0.0346	2.3	0.0373	-7.4
R 32	7944.802	12	11.63	0.0310	3.2	0.0311	-0.1
R 34	7946.156	10	10.0	0.0271	2.5	0.0253	7.2
R 36	7947.501	10	5.22	0.0216	4.8	0.0203	6.6
R 38	7948.838	9	2.46	0.0160	7.1	0.0159	0.3
R 40	7950.167	8	2.67	0.0113	6.8	0.0123	-8.0
R 42	7951.490	3	0.32	0.0093	19.5	0.0093	0.3

[a]Line positions calculated from Mandin *et al.* (15).
[b]Number of measurements.
[c]Weight used in least-squares fit for band intensity parameters.
[d]Line intensity in units of 10^{-25} cm^{-1}/(molecule/cm^2) at 296K.
[e]Twice the standard deviation of the mean of S_{obs}, as percentage of S_{obs}.

the rovibrational partition function for $^{12}C^{16}O_2$ is $Q_{vr}(296) = 286.14$ (14), the square of the rotationless transition moment $|R_{vib}|^2$ has units of D^2, J'' is the lower state rotational quantum number, and $f = 0.9842$ is the isotopic fraction for $^{12}C^{16}O_2$. The lower state rotational energy values $E''(cm^{-1})$ were adopted from the HITRAN tabulations, and the vacuum line positions $\sigma(cm^{-1})$ were calculated from the rotational constants of Mandin (15). The Hönl–London linestrength factors $L_{J''}$ are equal to J'' and $(J'' + 1)$ respectively for the P and R branches of parallel ground state bands. T is the Kelvin temperature and k, h, and c have their usual definitions.

Solving Eq. [1] for $|R_{vib}|^2F(m)$, where $m = -J''$ and $J'' + 1$ in the P and R branches, respectively, we defined the reduced line intensity as $S_{red}(m) = |R_{vib}|^2F(m)$,

$$|R_{vib}|^2F(m) = \{3hc10^{36}/8\pi^3\sigma fL_{J''}\}\{S_{J''}Q_{vr}(T)\exp(E''hc/kT)\}. \quad [2]$$

Following Rothman *et al.* (6), the Herman–Wallis factor is

$$F(m) = [1 + A_1m + A_2m^2 + A_3m^3]^2 \quad [3]$$

for the P and R branches. To determine the band intensity parameters, we found that cubic fits to our data were no better than quadratic fits. Thus, we did weighted quadratic least-squares fits to the square root of the experimentally determined reduced intensities:

$$|R_{vib}|[1 + A_1m + A_2m^2] = [S_{red}(m)]^{1/2}. \quad [4]$$

As suggested by Malathy Devi *et al.* (16), the weight for each line in Tables 3 and 4 was usually assigned equal to the number of spectra on which it was measured. However, for some lines the standard deviation of the measurements exceeded a maximum acceptable value δ (expressed in percent) chosen for each band. These lines were weighted less than the lines with acceptable standard deviations; their weight was calculated as the square of the ratio of δ divided

TABLE 4
Rovibrational Line Intensities for the $(40^01)_{IV} \leftarrow (00^00)$ Band of $^{12}C^{16}O_2$

Line	$\sigma(cm^{-1})^a$	n[b]	wt[c]	S_{obs}[d]	$2\Delta S\%$[e]	S_{cal}[d]	$(S_{obs}-S_{cal})/S_{cal}$ (%)
P 42	7422.649	5	1.15	0.248	6.5	0.236	4.9
P 38	7426.733	1	1.0	0.398		0.389	2.4
P 36	7428.734	9	3.21	0.456	3.9	0.486	-6.3
P 34	7430.709	19	19.0	0.607	1.6	0.598	1.5
P 32	7432.658	13	13.0	0.695	1.7	0.722	-3.7
P 30	7434.581	19	19.0	0.866	1.3	0.855	1.4
P 28	7436.478	11	11.0	0.978	1.4	0.993	-1.5
P 26	7438.351	14	14.0	1.124	1.8	1.131	-0.7
P 24	7440.199	6	6.0	1.258	1.9	1.262	-0.3
P 22	7442.023	12	12.0	1.378	1.5	1.379	-0.0
P 20	7443.822	12	12.0	1.492	1.4	1.471	1.4
P 18	7445.598	11	11.0	1.536	2.1	1.531	0.3
P 16	7447.349	8	8.0	1.526	2.2	1.552	-1.7
P 14	7449.078	10	7.36	1.540	2.6	1.525	1.0
P 12	7450.783	10	10.0	1.435	1.6	1.447	-0.8
P 10	7452.464	8	5.09	1.307	3.1	1.314	-0.6
P 8	7454.123	14	14.0	1.145	1.3	1.131	1.2
P 6	7455.758	19	19.0	0.912	1.0	0.898	1.5
P 4	7457.371	19	19.0	0.637	1.3	0.624	2.0
P 2	7458.960	15	15.0	0.322	1.2	0.321	0.3
R 0	7461.302	4	2.72	0.162	4.2	0.163	-0.5
R 2	7462.834	17	10.82	0.494	2.1	0.484	2.1
R 4	7464.343	10	7.60	0.797	2.5	0.788	1.2
R 6	7465.829	16	16.0	1.026	1.1	1.062	-3.4
R 8	7467.292	13	13.0	1.292	1.3	1.295	-0.3
R 10	7468.731	8	8.0	1.489	1.6	1.479	0.6
R 12	7470.147	10	10.0	1.597	1.6	1.610	-0.8
R 14	7471.539	10	10.0	1.697	1.2	1.686	0.7
R 16	7472.907	10	10.0	1.703	1.8	1.708	-0.3
R 18	7474.251	9	9.0	1.696	2.0	1.681	0.9
R 20	7475.571	10	10.0	1.588	1.9	1.615	-1.6
R 22	7476.866	7	7.0	1.506	1.7	1.511	-0.4
R 24	7478.136	12	12.0	1.356	2.0	1.385	-2.1
R 26	7479.380	11	11.0	1.205	2.1	1.242	-3.0
R 28	7480.599	13	13.0	1.072	1.5	1.092	-1.8
R 30	7481.792	19	19.0	0.963	1.5	0.942	2.3
R 32	7482.958	14	14.0	0.785	1.5	0.797	-1.5
R 34	7484.098	14	14.0	0.670	1.4	0.661	1.3
R 36	7485.210	2	2.0	0.553	4.4	0.540	2.4
R 38	7486.294	16	11.46	0.431	2.1	0.432	-0.4
R 40	7487.349	17	17.0	0.343	1.4	0.340	0.7
R 42	7488.376	18	9.87	0.262	2.2	0.264	-0.6
R 44	7489.373	8	2.85	0.202	4.1	0.201	0.7
R 46	7490.341	11	6.57	0.153	2.7	0.150	1.6
R 48	7491.277	5	0.73	0.115	8.2	0.111	4.4

[a]Line positions calculated from Mandin *et al.* (15).
[b]Number of measurements.
[c]Weight used in least-squares fit for intensity parameters.
[d]Line intensity in units of 10^{-25} cm^{-1}/(molecule/cm^2) at 296K.
[e]Twice the standard deviation of the mean of S_{obs}, as percentage of S_{obs}.

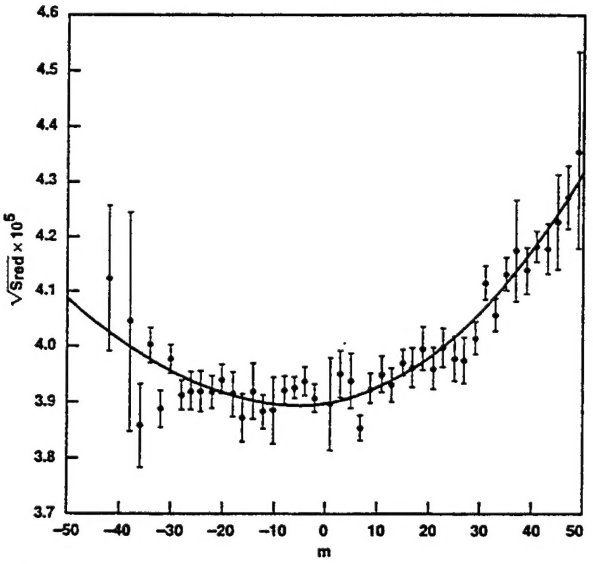

FIG. 3. Weighted quadratic least-squares fit of $[S_{red}(m)]^{1/2}$ for the $(40^01)_{IV} \leftarrow (00^00)$ band to determine $|R_{vib}|$, $|R_{vib}|A_1$, and $|R_{vib}|A_2$.

by the standard deviation of the mean (expressed in per cent) found in Tables 3 and 4. We chose $\delta = 5.55$ for Table 3 and $\delta = 3.48$ for Table 4.

These fits of the data for each band to Eq. [4] returned values and standard errors for $|R_{vib}|$ and the product parameters $|R_{vib}|A_1$ and $|R_{vib}|A_2$. Figures 3 and 4 show the result of fitting the square root of our reduced experimental intensities vs m. The error bars on these figures are $(\Delta S\%/100)[S_{red}(m)]^{1/2}$, where the $\Delta S\%$ are half the values listed in column 6 of Tables 3 and 4. The intensity parameters obtained from these fits are presented in Table 5.

The rotationless band strengths S^0_{vib}, as used in the 1992 HITRAN (6) tabulation, were evaluated at 296 K from these values of the rotationless transition moment of these ground state bands,

$$S^0_{vib}(T) = \{8\pi^3 10^{-36}/[3hcQ_v(T)]\}\sigma_0 f|R_{vib}|^2, \qquad [5]$$

using the value of the vibrational partition function $Q_v(296\ K) = 1.0846$ from Gray and Young (14), and the appropriate vibrational band origin, $\sigma_0 = 7920.838$ and $7460.527\ cm^{-1}$ respectively for bands I and IV of the pentad. These results are included in Table 5.

The uncertainties for the values of $|R_{vib}|$ were computed by two different methods and the larger uncertainty was adopted. In the first method, the standard errors for the $|R_{vib}|$ values were produced by the quadratic fitting procedure for the averaged S_{red} values as shown in Figs. 3 and 4. Since this method may overlook uncertainties in the laboratory conditions of each spectrum, we also determined $|R_{vib}|$ values from fits for 12 individual spectra for the $(40^01)_I \leftarrow (00^00)$ band and 11 spectra for the $(40^01)_{IV} \leftarrow (00^00)$ band. These values were then averaged for each band and the standard deviation of the mean calculated. The line intensity measurement errors are the major source of uncertainty for the weaker band; the goodness of fit in Fig. 4 for the weak $(40^01)_I \leftarrow (00^00)$ band is much less than that in Fig. 3 for the $(40^01)_{IV} \leftarrow (00^00)$ band. Uncertainties in the laboratory conditions, on the other hand, have a nearly equal effect on both bands. As a result, in Table 5 the uncertainty of $|R_{vib}|$ for the $(40^01)_I \leftarrow (00^00)$ band is twice the standard error from the quadratic fit, while for the $(40^01)_{IV} \leftarrow (00^00)$ band it is twice the standard deviation of the mean calculated from the second method.

The uncertainties in Table 5 for the quantities $|R_{vib}|A_1$ and $|R_{vib}|A_2$ are the standard errors from the quadratic fitting procedure. The values of A_1 and A_2 and their uncertainties were then obtained by dividing $|R_{vib}|A_1$ and $|R_{vib}|A_2$ by $|R_{vib}|$. Since the percentage uncertainties of the $|R_{vib}|$ values are much smaller than those of $|R_{vib}|A_1$ and $|R_{vib}|A_2$, the uncertainties of A_1 and A_2 shown in Table 5 have almost no dependence on the $|R_{vib}|$ uncertainties. However, the determination of A_2 is quite sensitive to the experimental temperature uncertainties. All the spectra were obtained with the metal White cells at room temperature; the temperature inside is within 1 K of the temperature outside. To determine the dependence of A_2 on the temperature, we repeated the quadratic fits of the S_{red} data for both bands assuming a systematic temperature difference of 1 K. This resulted in

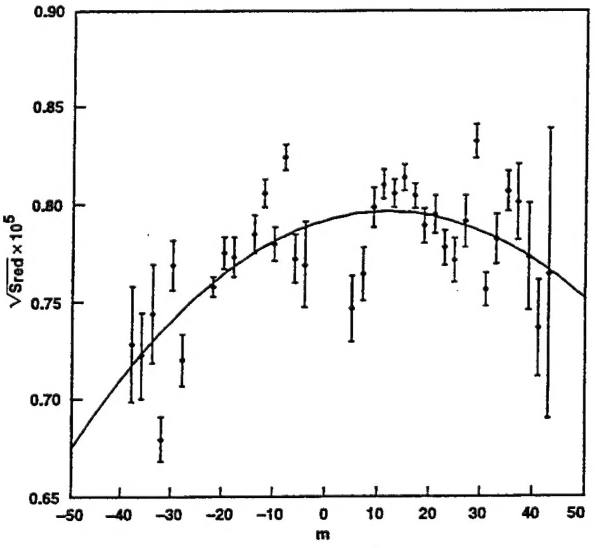

FIG. 4. Weighted quadratic least-squares fit of $[S_{red}(m)]^{1/2}$ for the $(40^01)_I \leftarrow (00^00)$ band to determine $|R_{vib}|$, $|R_{vib}|A_1$, and $|R_{vib}|A_2$.

TABLE 5
Intensity Parameters for the 7921 and 7460 cm^{-1} Bands of $^{12}C^{16}O_2$

Parameter	$(40^01)_{II}\leftarrow(00^00)$ Band	$(40^01)_{IV}\leftarrow(00^00)$ Band
$\lvert R_{vib}\rvert$	$(7.95\pm0.12)\times10^{-6}$ D	$(3.902\pm0.029)\times10^{-5}$ D
$\lvert R_{vib}\rvert A_1$	$(8.3\pm1.8)\times10^{-9}$	$(1.78\pm0.23)\times10^{-8}$
$\lvert R_{vib}\rvert A_2$	$(-3.65\pm.98)\times10^{-10}$	$(11.3\pm1.0)\times10^{-10}$
$^a\lvert R_{vib}\rvert^2$	$(6.32\pm0.20)\times10^{-11}$ D^2	$(1.523\pm0.023)\times10^{-9}$ D^2
$^bA_1$	0.00104±0.00023	0.00046±0.00006
$^bA_2$	$(-4.6\pm1.3)\times10^{-5}$	$(2.9\pm0.5)\times10^{-5}$
$^cS^0_{vib}$	$(0.189\pm0.006)\times10^{-24}$	$(4.29\pm0.06)\times10^{-24}$

[a] $\lvert R_{vib}\rvert^2$ is the rotationless transition moment squared in units of Debye^2.
[b] The A_1 and A_2 Herman-Wallis parameters are dimensionless.
[c] The units of S^0_{vib} are $cm^{-1}/(molecule/cm^2)$ at 296K.

A_2 values for both bands that differ from the values in Table 5 by 0.3×10^{-5}. This additional amount was then included in the uncertainty for the A_2 values. The percentage uncertainties for the values of $|R_{vib}|^2$ and S^0_{vib} in Table 5 were set equal to twice those of the $|R_{vib}|$ values, as is appropriate when squaring a quantity.

The line positions tabulated in Tables 3 and 4 were calculated from the rotational constants given by Mandin (15) and agree with the positions of those lines that are sufficiently intense to be included in the HITRAN tabulation (6). The 2–0 vibrational band of CO provided calibration line positions (17) on the Kitt Peak spectrum of the $(40^01)_{IV} \leftarrow (00^00)$ CO_2 band (see Table 2). The CO_2 line positions determined from our fits of this spectrum averaged about 0.005 cm^{-1} less than the HITRAN line positions. This difference is well within the HITRAN uncertainty limits of 0.01 to 0.1 cm^{-1} for these line positions; we conclude from our limited set of calibrated line position measurements that the HITRAN positions are at least as accurate as claimed.

DISCUSSION

The intensities and Herman–Wallis parameters for the pentad bands on the HITRAN listing in Table 1 are a mixture of values based on laboratory measurements and on DND calculations. The intensities of the $(40^01)_{II} \leftarrow (00^00)$ and $(40^01)_{III} \leftarrow (00^00)$ bands are based on the measurements of Valero and Boese (7) and Valero (8); these two band intensities were included by Wattson and Rothman (9) in their calculation of the dipole-moment function for DND. Therefore, the HITRAN parameters calculated by DND for the other three pentad bands have some dependence on the intensities of the two previously measured bands.

The intensities of the $(40^01)_I \leftarrow (00^00)$ and $(40^01)_{IV} \leftarrow (00^00)$ bands measured on our spectra are within 10% of the HITRAN calculated intensities. The calculated intensities were revisions by about 20% of the values in the 1986 HITRAN listing of Rothman (13). Both the 1986 and 1992 HITRAN databases used DND calculations for the band intensity parameters for these two bands. The differences in the two compilations are due to a more complete dipole-moment model and more accurate weighting of observed data in the DND calculations for the 1992 HITRAN compilation. This resulted in decreasing the calculated intensity for the $(40^01)_I \leftarrow (00^00)$ band and increasing it for the $(40^01)_{IV} \leftarrow (00^00)$ band. Surprisingly, our measured intensities for both bands lie about halfway between the calculated intensities in these two tabulations.

The Herman–Wallis parameters that we determined in Table 5 can also be compared to the calculated 1992 HITRAN values in Table 1 for the $(40^01)_I \leftarrow (00^00)$ and $(40^01)_{IV} \leftarrow (00^00)$ bands, since the DND calculated parameters were listed for unmeasured bands. Our measured A_2 coefficient of $(2.9 \pm 0.5) \times 10^{-5}$ for the $(40^01)_{IV} \leftarrow (00^00)$ band is in excellent agreement with the DND calculated value of 2.82×10^{-5}. Our measured A_2 value of $(-4.6 \pm 1.3) \times 10^{-5}$ for the weak $(40^01)_I \leftarrow (00^00)$ band has much greater uncertainty, but confirms the DND calculation that A_2 is negative. The DND calculations for all these $n\nu_1 + \nu_3$ polyads show A_2 varying smoothly from a negative value for the first (highest wavenumber) member to the highest positive value for the final (lowest wavenumber) member.

TABLE 6
Revised Parameters for the 7734 and 7594 cm^{-1} Bands of $^{12}C^{16}O_2$

Parameter	$(40^01)_{II}\leftarrow(00^00)$ Band	$(40^01)_{III}\leftarrow(00^00)$ Band
$\lvert R_{vib}\rvert$	$(3.181\pm0.020)\times10^{-5}$ D	$(6.02\pm0.07)\times10^{-5}$ D
$\lvert R_{vib}\rvert A_1$	$(9.8\pm2.7)\times10^{-9}$	$(7.3\pm10.4)\times10^{-9}$
$\lvert R_{vib}\rvert A_2$	$(-9.0\pm1.3)\times10^{-10}$	$(-5.4\pm4.9)\times10^{-10}$
$^a\lvert R_{vib}\rvert^2$	$(1.012\pm0.013)\times10^{-9}$ D^2	$(3.62\pm0.09)\times10^{-9}$ D^2
$^bA_1$	0.00031±0.00008	0.00012±0.00017
$^bA_2$	$(-2.8\pm0.4)\times10^{-5}$	$(-0.9\pm0.8)\times10^{-5}$
$^cS^0_{vib}$	$(2.96\pm0.04)\times10^{-24}$	$(10.38\pm0.26)\times10^{-24}$

[a] $\lvert R_{vib}\rvert^2$ is the rotationless transition moment squared in units of Debye^2.
[b] The A_1 and A_2 Herman-Wallis parameters are dimensionless.
[c] The units of S^0_{vib} are $cm^{-1}/(molecule/cm^2)$ at 296K.

TABLE 7

Some $(40^01)_i \leftarrow (00^00)$ Pentad Band Intensity Parameters Determined in This Work[a] Divided by Corresponding Parameters Taken from Table 1[b]

i	S^0_{vib}(this)/S^0_{vib}(HITRAN)	A_1(this)/A_1(HITRAN)	A_2(this)/A_2(HITRAN)
I	1.08	1.39	1.89
II	1.05	1.24	c
III	1.02	c	c
IV	0.91	-3.29	1.03

[a]See Tables V and VI.
[b]1992 HITRAN (Ref. 6).
[c]Not determined.

As for A_1, our measured value of $(1.04 \pm 0.23) \times 10^{-3}$ for the $(40^01)_I \leftarrow (00^00)$ band agrees well with the calculated value of 0.75×10^{-3}, but the DND calculation for the $(40^01)_{IV} \leftarrow (00^00)$ band expects A_1 to be small and negative, whereas our measured value is $A_1 = (4.6 \pm 0.6) \times 10^{-4}$.

Valero and Boese (7) first fit their line intensity measurements with a linear least-squares and thus did not determine a quadratic Herman–Wallis factor for the $(40^01)_{II} \leftarrow (00^00)$ band. Arie *et al.* (18) reanalyzed these measurements using a quadratic fit, assuming that $A_1 = 0$. This motivated Valero and Boese (10) to reanalyze their measurements using a quadratic least-squares fit to determine both linear and quadratic Herman–Wallis parameters; this fit increased the intensity of the band by several percent compared to their original linear fit. However, the HITRAN parameters for this band are based only on the original paper and did not incorporate either of these subsequent quadratic fits; hence, HITRAN assigned $A_2 = 0$ for this band. Valero (8) then used a similar quadratic least squares fit for his line intensity measurements of the $(40^01)_{III} \leftarrow (00^00)$ band to obtain the band intensity and both Herman–Wallis parameters. His band intensity was adopted for the HITRAN tabulations; however, Rothman *et al.* (6) assigned both $A_1 = 0$ and $A_2 = 0$ for this band.

Since the prior fits for the line intensities of these two bands all used expressions for $F(m)$ that differed slightly from Eq. [3], we reduced the measurements of Valero and Boese (7) and Valero (8) using the same procedure as discussed above for our own measurements. These articles (7, 8) tabulate their line intensities through $J'' = 40$, which were determined from equivalent width measurements and reduced to line intensities using the CO_2 self-broadening coefficients of Yamamoto *et al.* (19). These self-broadening values agree with the recent formulation of Rothman *et al.* (6) within 6% over $J'' = 0$ through 40. Were it possible to redetermine their line intensities using the new values of self-broadening coefficients, we estimate that these intensity values would change by less than 2%, which is within the uncertainties of their individual line equivalent width measurements.

We made plots for the $(40^01)_{II} \leftarrow (00^00)$ and $(40^01)_{III} \leftarrow (00^00)$ bands that are similar to Figs. 3 and 4 and determined $|R_{vib}|$, $|R_{vib}|A_1$, and $|R_{vib}|A_2$ from quadratic least-squares fits. The fits for these bands were not weighted, since the number of measurements for each line were not available from Valero and Boese (7) and Valero (8). Our plot for the $(40^01)_{II} \leftarrow (00^00)$ band had the same appearance as the plot of the same data by Arie *et al.* (18). We omitted the $R(0)$ line for this fit, since its measured intensity was nearly 20% less than its calculated value, making it several times more discordant than any other line. The parameters we determined and their corresponding uncertainties are given in Table 6 and agree with the values of $|R_{vib}|$, A_1, and A_2 determined in the refit of Valero and Boese (10) when their linear and quadratic fitting parameters are converted to Herman–Wallis parameters as defined by Eq. [3]. Our band intensity value S^0_{vib}[II] is 5% larger than the value in Rothman *et al.* (6), which was based on the original linear fit of Valero and Boese (7).

The parameters determined from our fit of Valero's (8) data for the $(40^01)_{III} \leftarrow (00^00)$ band are also listed in Table 6. Our band intensity value S^0_{vib}[III] is only 2% larger than the HITRAN value which was based on Valero's (8) results. The Herman–Wallis parameters we determined for this band have uncertainties of about the same magnitude; therefore, HITRAN's assignment of zero for these parameters is not unreasonable. Despite the close agreement for the band intensity, our value of $|R_{vib}|$ disagrees with Valero's (8) by more than a factor of 3. We believe he actually fit $|R_{vib}|^2$ and his value of S_{Band} correctly from his line intensity data, but miscalculated $|R_{vib}|$ from $|R_{vib}|^2$.

All these comparisons between intensity parameters determined in this paper for the $(40^01)_i \leftarrow (00^00)$ pentad bands (i

= I, II, III, IV) and those given by the 1992 HITRAN database are summarized as ratios in Table 7.

Having now determined consistent intensities and Herman–Wallis parameters for the first four bands of the $(40^01) \leftarrow (00^00)$ pentad, we note that the A_2 Herman–Wallis parameter changes consistently from a negative value for the first member of the pentad to a positive value for the fourth member. In particular, we find that the value for the second and fourth bands are of opposite sign and nearly equal magnitude. This is consistent with the DND-calculated A_2 parameters for bands of all these $n\nu_1 + \nu_3$ polyads, as are the measured A_2 values for the dyad bands given in Table 1. However, the 1992 HITRAN values of A_2 for the triad and tetrad bands do not agree with DND calculations. The Herman–Wallis parameters for the triad and tetrad bands are based on prior measurements; all the A_2 parameters for the $3\nu_1 + \nu_3$ tetrad bands in Table 1 have positive values, whereas DND calculations of A_2 show systematic changes for the triad and tetrad bands similar to the trends found for the dyad and pentad.

To check the old measured A_2 values, we have made preliminary line intensity measurements of the $(30^01)_I \leftarrow (00^00)$ and $(30^01)_{IV} \leftarrow (00^00)$ bands on the same two spectra obtained at Kitt Peak on which we measured self-broadening coefficients. Reductions of these new data show a negative value of A_2 for the $(30^01)_I \leftarrow (00^00)$ band and a positive value for the $(30^01)_{IV} \leftarrow (00^00)$ band, in agreement with measurements done by Toth *et al.* (20); this is consistent with the DND calculations for these bands and also consistent with the trend of the measured values for the dyad and pentad bands. The discrepancy found between our new measurements and the 1992 HITRAN values, which are based on the measurements of Suarez and Valero (21) for the tetrad bands, will be investigated fully when additional spectra are measured.

CONCLUSION

Our new measurements of two bands and the refitting of prior measurements of two other bands provide statistically well-determined band intensities and Herman–Wallis parameters for the first four of the pentad bands of $^{12}C^{16}O_2$ between 7284 and 7921 cm^{-1}. We recommend that these values be considered for the next update of the HITRAN database. These new measurements and analyses have confirmed the DND intensity calculations to within about 10% for the two pentad bands not previously measured. This is regarded as good agreement, since DND is not expected to give exact intensity parameters for unmeasured ground state, principal isotopomer bands, as not enough information is available to accurately determine the dipole-moment surface. However, our measurements encourage us to believe that the DND intensity parameters for unmeasured bands of a polyad are reasonably accurate when based on calculations that include measured intensities of other bands of the same polyad. Thus, we expect that the current 1992 HITRAN intensity value for the still unmeasured $(40^01)_V \leftarrow (00^00)$ band at 7284 cm^{-1} is accurate to about 10%.

ACKNOWLEDGMENTS

The importance of improving the intensity values of the CO_2 bands near 7900 cm^{-1} for modeling Venus spectra was suggested by James B. Pollack. Richard S. Freedman provided helpful listings of HITRAN and DND-calculated comparison spectra. The referee provided a number of helpful comments for improving the manuscript. Part of the research reported in this paper was performed at the Jet Propulsion Laboratory, California Institute of Technology, under contract with the National Aeronautics and Space Administration.

REFERENCES

1. D. A. Allen, *Icarus* **69,** 221–229 (1987); *Int. Astron. Union Cir.* **4962** (1990).
2. B. Bézard, C. de Bergh, D. Crisp, and J.-P. Maillard, *Nature* **345,** 508–511 (1990).
3. R. W. Carlson, K. H. Baines, Th. Encrenaz, F. W. Taylor, P. Drossart, L. W. Kamp, J. B. Pollack, E. Lellouch, A. D. Collard, S. B. Calcutt, D. Grinspoon, P. R. Weissman, W. D. Smythe, A. C. Ocampo, G. E. Danielson, F. P. Fanale, T. V. Johnson, H. H. Kieffer, D. L. Matson, T. McCord, and L. A. Soderblom, *Science* **253,** 1541–1548 (1991).
4. J. B. Pollack, J. B. Dalton, D. Grinspoon, R. B. Wattson, R. Freedman, D. Crisp, D. A. Allen, B. Bezard, C. DeBergh, L. P. Giver, Q. Ma, and R. Tipping, *Icarus* **103,** 1–42 (1993).
5. L. P. Giver and C. Chackerian, Jr., *J. Mol. Spectrosc.* **148,** 80–85 (1991).
6. L. S. Rothman, R. L. Hawkins, R. B. Wattson, and R. R. Gamache, *J. Quant. Spectrosc. Radiat. Transfer* **48,** 537–566 (1992).
7. F. P. J. Valero and R. W. Boese, *J. Quant. Spectrosc. Radiat. Transfer* **18,** 391–398 (1977).
8. F. P. J. Valero, *J. Mol. Spectrosc.* **68,** 269–279 (1977).
9. R. B. Wattson and L. S. Rothman, *J. Quant. Spectrosc. Radiat. Transfer* **48,** 763–780 (1992).
10. F. P. J. Valero and R. W. Boese, *J. Quant. Spectrosc. Radiat. Transfer* **20,** 427 (1978).
11. J. U. White, *J. Opt. Soc. Am.* **32,** 285–288 (1942).
12. M. N. Spencer, C. Chackerian, Jr., L. P. Giver, and L. R. Brown, *J. Mol. Spectrosc.* **165,** 506–524 (1994).
13. L. S. Rothman, *Appl. Opt.* **25,** 1795–1816 (1986).
14. L. D. Gray and A. T. Young, *J. Quant. Spectrosc. Radiat. Transfer* **9,** 569–589 (1969).
15. J.-Y. Mandin, *J. Mol. Spectrosc.* **67,** 304–321 (1977).
16. V. Malathy Devi, C. P. Rinsland, and D. C. Benner, *Appl. Opt.* **23,** 4067–4075 (1984).
17. C. R. Pollock, F. R. Petersen, D. A. Jennings, and J. S. Wells, *J. Mol. Spectrosc.* **99,** 357–368 (1983).
18. E. Arie, N. Lacome, and P. Arcas, *J. Quant. Spectrosc. Radiat. Transfer* **20,** 425–426 (1978).
19. G. Yamamoto, M. Tanaba, and T. Aoki, *J. Quant. Spectrosc. Radiat. Transfer* **9,** 371–382 (1969).
20. R. A. Toth, R. H. Hunt, and E. K. Plyler, *J. Mol. Spectrosc.* **38,** 107–117 (1971).
21. C. B. Suarez and F. P. J. Valero, *J. Quant. Spectrosc. Radiat. Transfer* **19,** 569–578 (1978).